



Amino acid starvation-induced LDLR trafficking accelerates lipoprotein endocytosis and LDL clearance

Ye Chen^{1,2,†}, Xiao Wu^{1,3,4,†} , Jing Zhang¹, Guopin Pan¹, Xiaoyun Wang¹, Xiaosun Guo¹, Jianli Wang⁵, Xiaopei Cui², Haiqing Gao², Mei Cheng², Jingwen Yang¹, Cheng Zhang^{3,4,*}  & Fan Jiang^{2,**} 

Abstract

Mammalian cells utilize Akt-dependent signaling to deploy intracellular Glut4 toward cell surface to facilitate glucose uptake. Low-density lipoprotein receptor (LDLR) is the cargo receptor mediating endocytosis of apolipoprotein B-containing lipoproteins. However, signaling-controlled regulation of intracellular LDLR trafficking remains elusive. Here, we describe a unique amino acid stress response, which directs the deployment of intracellular LDLRs, causing enhanced LDL endocytosis, likely via Ca²⁺ and calcium/calmodulin-dependent protein kinase II-mediated signalings. This response is independent of induction of autophagy. Amino acid stress-induced increase in LDL uptake *in vitro* is comparable to that by pravastatin. *In vivo*, acute AAS challenge for up to 72 h enhanced the rate of hepatic LDL uptake without changing the total expression level of LDLR. Reducing dietary amino acids by 50% for 2 to 4 weeks ameliorated high fat diet-induced hypercholesterolemia in heterozygous *LDLR*-deficient mice, with reductions in both LDL and VLDL fractions. We suggest that identification of signaling-controlled regulation of intracellular LDLR trafficking has advanced our understanding of the LDLR biology, and may benefit future development of additional therapeutic strategies for treating hypercholesterolemia.

Keywords amino acid starvation; calcium signaling; endocytic recycling; endocytosis; low-density lipoprotein receptor

Subject Categories Membranes & Trafficking; Metabolism

DOI 10.15252/embr.202153373 | Received 2 June 2021 | Revised 15 December 2021 | Accepted 21 December 2021 | Published online 7 January 2022

EMBO Reports (2022) 23: e53373

Introduction

Low-density lipoprotein receptor (LDLR) is the cargo receptor mediating cellular uptake of apolipoprotein B-containing lipoproteins, such as LDL and very low-density lipoprotein (VLDL) (Goldstein & Brown, 2009; van de Sluis *et al.*, 2017). Mutations in LDLR have been identified as the cause of familial hypercholesterolemia (van de Sluis *et al.*, 2017). Ligand engagement with LDLR triggers clathrin-mediated endocytosis of the ligand-receptor complex, and the LDLR is then dissociated from the ligand in early (sorting) endosomes. The internalized lipoprotein particles are subsequently delivered to late endosomes and finally to lysosomes for degradation. Inside the early endosome (EE), LDLRs can either enter the recycling process, thereby are sent back to the plasma membrane (PM) for reuse, or be sorted to the lysosome compartment for degradation (Wijers *et al.*, 2015). Because of the pivotal role of LDLR in clearing atherogenic lipoproteins from the circulation, there are tremendous successes in drug development by targeting LDLR, exemplified by the discovery of statins (3-hydroxy-3-methyl-glutaryl-coenzyme A reductase inhibitors) and proprotein convertase subtilisin/kexin type 9 (PCSK9) inhibitors, both of which can increase the LDLR protein availability by promoting LDLR gene expression and suppressing LDLR protein degradation, respectively (Mourikis *et al.*, 2020).

The internalized LDLRs return to PM either directly via the “fast pathway” or indirectly via the “slow pathway” (Maxfield & McGraw, 2004; Grant & Donaldson, 2009; Naslavsky & Caplan, 2018). In the former, vesicles containing the receptors bud off from EE and undergo transport directly to PM (Naslavsky & Caplan, 2018); this process requires small G proteins Rab4 and Rab35 (Grant & Donaldson, 2009; Stenmark, 2009). The latter encompasses *en route* more specialized recycling endosomes (REs) (also termed the

1 Department of Physiology and Pathophysiology, School of Basic Medical Sciences, Cheeloo College of Medicine, Shandong University, Jinan, China
2 Key Laboratory of Cardiovascular Proteomics of Shandong Province, Department of Geriatrics, Qilu Hospital, Cheeloo College of Medicine, Shandong University, Jinan, China
3 Key Laboratory of Cardiovascular Remodeling and Function Research, Chinese Ministry of Education, Chinese National Health Commission and Chinese Academy of Medical Sciences, Jinan, China

4 The State and Shandong Province Joint Key Laboratory of Translational Cardiovascular Medicine, Department of Cardiology, Qilu Hospital of Shandong University, Jinan, China

5 Department of Obstetrics and Gynecology, Qilu Hospital of Shandong University, Jinan, China

*Corresponding author. Tel: +86 531 8216 9257; Fax: +86 531 8616 9356; E-mail: zhangc@sdu.edu.cn

**Corresponding author. Tel: +86 531 8216 6562; Fax: +86 531 8692 7544; E-mail: fjiang@sdu.edu.cn

†These authors contributed equally to this work

[Correction added on 12th January 2022, after first online publication: The copyright line was changed.]

endocytic recycling compartment/ERC), which are perinuclear-localized tubular clusters, adjacent to the microtubule-organizing center (Naslavsky & Caplan, 2018). The mechanisms of slow recycling appear to be divergent and are not yet completely understood (Grant & Donaldson, 2009; Naslavsky & Caplan, 2018). Nevertheless, it is well established that Rab11 is crucial for the slow recycling pathway via REs (Grant & Donaldson, 2009; Stenmark, 2009). Given the critical role of endocytic recycling in determining the fate of internalized receptors, it is anticipated that a better understanding of the regulation of LDLR recycling may provide additional therapeutic targets to treat hypercholesterolemia (Wijers *et al*, 2015).

Amino acid homeostasis is vital for maintaining normal cellular metabolism and growth, primarily via regulation of the mTORC1 (mammalian target of rapamycin complex 1) pathway (Jewell & Guan, 2013). The intracellular availability of free amino acids is mainly maintained by cross-membrane transport of amino acids from the extracellular environment into cells through various SLC (solute carrier) transporters (Carroll *et al*, 2015). Studies in both human beings and animal models have also suggested that pan-restriction of dietary intake of amino acids or reduced intake of certain amino acid(s) may have significant impacts on the systemic metabolic status *in vivo* (Karusheva *et al*, 2019; Yu *et al*, 2021), including lipid metabolism (Anthony *et al*, 2013). Interestingly, it was observed that reducing threonine intake decreased the level of serum triglyceride in obese mice (Yap *et al*, 2020). In addition, dietary protein restriction without enforced calorie restriction lowered the VLDL levels in both lean and obese mice (Treviño-Villarreal *et al*, 2018).

Under the condition of amino acid starvation (AAS), cells initiate autophagy, a conserved nutrient stress response involving membranous vesicle-mediated transfer of intracellular proteins and organelles to lysosomes for degradation, by which free amino acids are released into the cytoplasm for reutilization (Ravikumar *et al*, 2010; Carroll *et al*, 2015). Intuitively, however, cells should be equipped with additional apparatuses to acquire nutrients from alternative extracellular sources to deal with the stress condition, even before starting to digest intracellular components. For this purpose, lipoprotein particles, such as low-density lipoprotein (LDL) and very low-density lipoprotein (VLDL), may be an ideal candidate. LDL uptake is a crucial route of cholesterol supply for steroid hormone biosynthesis in adrenocortical and gonadal tissues (Hu *et al*, 2010). In cells where endogenous cholesterol synthesis is blocked, the cells rely on endocytosis of exogenous LDL as the source of cholesterol for maintaining membrane integrity (Goldstein & Brown, 2009). Supporting our hypothesis, emerging evidence shows that certain tumor cells can survive the nutrient-poor microenvironment by activating endocytosis of extracellular macromolecules as the source of amino acids (Xiao *et al*, 2020). Moreover, it is known that, at least in hepatocytes, the protein components of internalized lipoprotein molecules are degraded by the lysosome system, releasing free amino acids (Heeren & Beisiegel, 2001).

It is known that cellular uptake of glucose may be stimulated by insulin in an acute manner through regulated trafficking of intracellular vesicles containing the glucose transporter Glut4, a response mediated by tyrosine phosphorylation of the adaptor protein c-CBL and/or activation of the serine-threonine kinase Akt (Bryant *et al*, 2002; Leto & Saltiel, 2012). However, a comparable signal transduction mechanism that can control the trafficking of LDLRs has not yet

been reported. In this study, we describe a novel phenomenon in which AAS induces a quick response of deployment of intracellular LDLRs to PM, leading to increased surface LDLR availability and enhanced lipoprotein endocytosis. To our knowledge, this response has not been reported previously. Moreover, this mechanism is found to be functional *in vivo*.

Results

AAS increases LDLR-dependent lipoprotein endocytosis

We incubated NIH-3T3 cells in the complete medium and mediums containing 50% and 0% of the normal level of amino acids, together with supplemented DiI-LDL, observed with fluorescence microscopy, and found that AAS accelerated LDL uptake in a time-dependent manner (Fig 1A). This response was reproduced in human HepG2 hepatocytes (Fig 1A). The increases in DiI-LDL uptake in AAS-treated cells were observed as early as 15 min. Using fixed time intervals of incubation, we determined that this AAS-induced response exhibited a “dose-response” relationship, since the medium containing 75% of amino acids had no effect (Appendix Fig S1). We also measured intracellular levels of DiI-LDL using flow cytometry, which confirmed our findings with fluorescence microscopy (Fig 1B). To further confirm the specificity of the response induced by AAS medium, we performed reversal experiments by adding exogenous amino acids to the medium, and showed that the increase in LDL uptake stimulated by AAS medium was abolished by amino acid replenishment (Fig 1C). In addition, we showed that deprivation of glucose or serum did not trigger a similar response as AAS (Fig 1D). Next, we performed competitive inhibition experiments by co-incubating the cells with an excessive amount of unlabeled LDL. It was demonstrated that unlabeled LDL abrogated AAS-induced DiI accumulation (Fig 1E), verifying that the intracellular DiI fluorescence reflected the internalized LDL particles. Moreover, we directly measured the cholesterol concentrations and showed that AAS significantly increased the cellular cholesterol content (Appendix Fig S2). To clarify whether AAS-stimulated LDL uptake was dependent on LDLR, we cultured hepatocytes and SVF from LDLR^{-/-} mouse. In contrast to WT cells, AAS-induced LDL endocytosis were virtually abolished in LDLR^{-/-} cells, although our data could not completely exclude the involvement of other receptor systems in mediating the low-level LDL internalization in LDLR^{-/-} cells (Fig 1F). Finally, to directly monitor the dynamics of LDL endocytosis, we pretreated the cells with AAS and arrested the endocytic process by chilling the cells at 4°C. Then the cells were fed with DiI-LDL and concomitantly returned to 37°C. The initial phase of intracellular DiI accumulation over 2 min was monitored using a fluorescence microplate reader. As shown in Fig 1G, the net rate of DiI internalization was higher in AAS-pretreated cells, supporting an increase in the volume of LDL endocytosis.

AAS-induced lipoprotein uptake is mediated by conventional clathrin-dependent endocytosis but not related to autophagy

In both 3T3 and HepG2 cells, we demonstrated that AAS-stimulated LDL uptake was abolished by the clathrin inhibitor

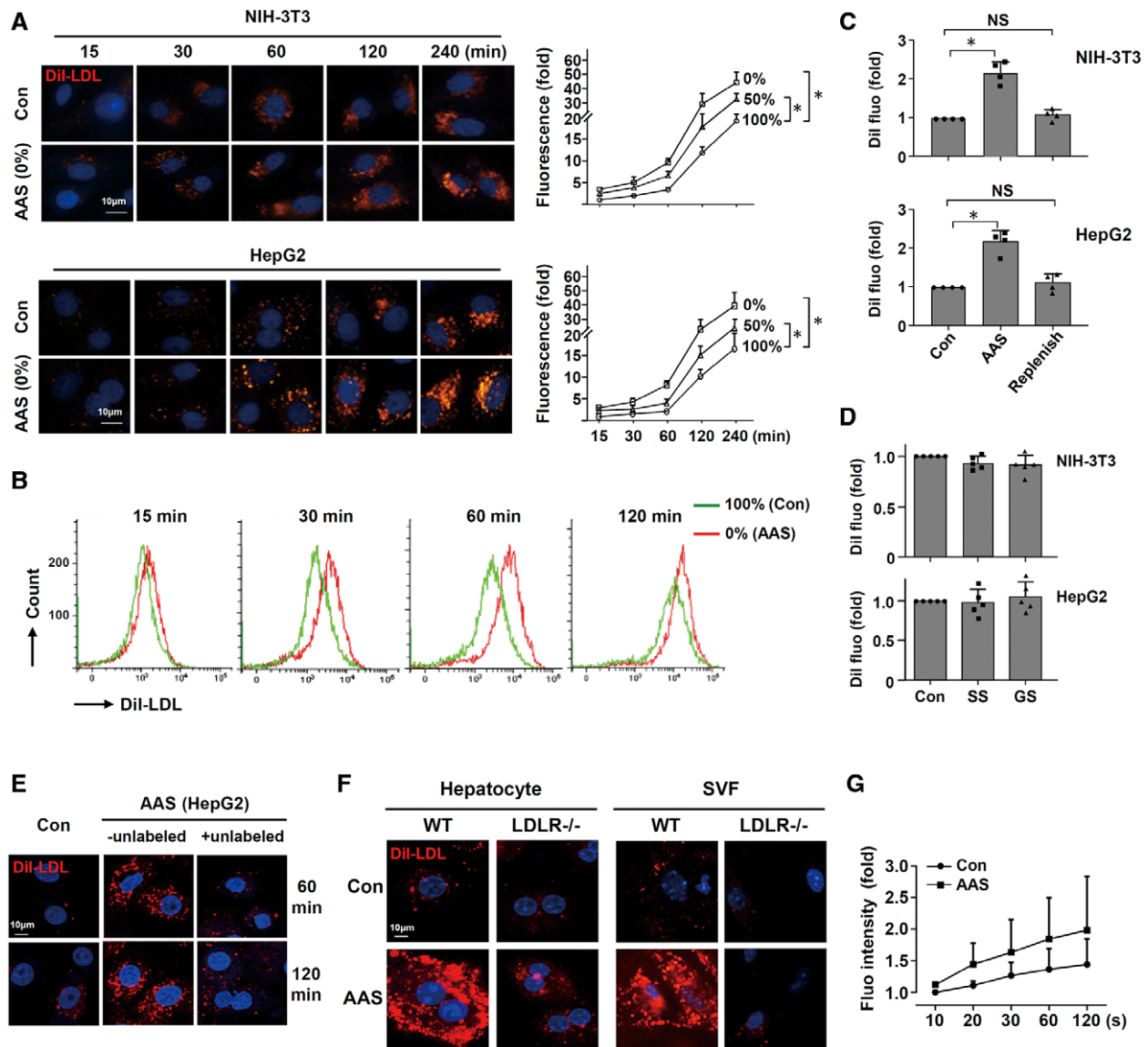


Figure 1. Acceleration of LDLR-dependent lipoprotein endocytosis in response to amino acid starvation (AAS).

- A Representative fluorescence microscopy images and quantitative data ($n = 4$ independent experiments) showing that reducing the extracellular concentration of amino acids to 50 and 0% of that in the complete culture medium (100%, Con) increased the rate of internalization of Dil-labeled LDL particles (10 $\mu\text{g}/\text{ml}$) in NIH-3T3 and HepG2 cells. The time points represented the duration of Dil-LDL incubation with or without AAS. Cell nuclei were counterstained with DAPI.
- B Flow cytometry data showing that AAS accelerated Dil-LDL internalization in NIH-3T3 cells (example from 3 independent experiments with similar results).
- C Fluorescence microscopy data showing that re-addition of amino acids to the AAS medium (50%) abolished the effect on Dil-LDL uptake (assays performed at 60 min). Con, complete culture medium.
- D Fluorescence microscopy data showing that glucose starvation (GS) or serum starvation (SS) (treatment for 60 min) had no effect on Dil-LDL uptake.
- E Fluorescence microscopy images (example from 3 independent experiments with similar results) showing that competitive inhibition by co-incubating HepG2 cells with an excessive amount of unlabeled LDL (100 $\mu\text{g}/\text{ml}$) virtually abrogated AAS (50%) induced Dil-LDL accumulation.
- F Fluorescence microscopy images showing that AAS (50% for 60 min) failed to modify Dil-LDL uptake in LDLR^{-/-} murine hepatocytes and stromal vascular fraction (SVF) of adipose tissue in contrast to wild-type (WT) cells (example from 3 independent experiments with similar results). NB. Contrast was uniformly adjusted over the original images to make the faint background signals in KO cells more outstanding.
- G Increased volume of LDL endocytosis in AAS-treated cells measured by monitoring the initial phase of intracellular Dil accumulation over 2 min using a fluorescence microplate reader (mean data from 4 independent experiments). NIH-3T3 cells were pretreated with AAS (0%) and endocytosis arrested at 4°C. Then the cells were fed with Dil-LDL and concomitantly returned to 37°C.

Data information: All data were expressed as mean \pm SD. * $P < 0.05$, one-way ANOVA. NS, no significance. For all Figures throughout, the n number represented independent experiments but not technical replicates.

Source data are available online for this figure.

Pitstop2 and the dynamin inhibitor Dynasore (Fig EV1A). Since AAS is the prototype inducer of cell autophagy, we tested next whether AAS-induced lipoprotein uptake was associated with autophagy. In both NIH-3T3 and HepG2 cells, we showed that AAS could not induce autophagy by 2 h, although AAS for a longer time interval triggered autophagy (Appendix Fig S3A–C). Nevertheless, the difference in time course of the two responses did not support a correlation between AAS-stimulated LDL endocytosis and autophagy. Then we treated NIH-3T3 and HepG2 cells with the autophagy inducer rapamycin. Rapamycin readily induced autophagy in both cells, but failed to mimic the effects of AAS on LDL endocytosis (Fig EV1B and C). Moreover, we treated HepG2 cells with a siRNA targeting Atg5, which reduced the expression level of Atg5 protein, and attenuated the basal level of autophagy (Fig EV1D and Appendix Fig S4). However, the Atg5 siRNA exhibited no significant effect on AAS-stimulated LDL endocytosis (Fig EV1D).

AAS increases the cell surface LDLR availability independent of *de novo* gene expression

Preliminary experiments using surface biotinylation and pull-down indicated that only a minor fraction of LDLRs were located on PM (Fig 2A). Further analysis of the biotinylated PM fractions demonstrated that AAS significantly increased the amount of LDLRs on PM (Fig 2B). To confirm the results, we performed flow cytometry with nonpermeabilized cells, and demonstrated that AAS increased the abundance of LDLRs on the cell surface in NIH-3T3 (Fig 2C) and HepG2 cells (Appendix Fig S5). To verify that the detected PM surface LDLRs in AAS-treated cells participated in the endocytic turnover, NIH-3T3 cells were detached and incubated with complete or AAS medium in suspension. Then the cells were transferred to 4°C (which arrested the endocytic transport), pulse-labeled with unconjugated LDLR antibody, and returned to 37°C to resume endocytosis for 60 min in the presence of exogenous LDL. In this case, the internalized primary antibodies were inaccessible to the secondary antibody. Thereafter, the cells were labeled with FITC-conjugated secondary antibody at 4°C. It was found that the surface LDLR signal was virtually abolished in both control and AAS-treated cells in these experiments (Fig 2D). As a positive control, we showed that if a PE-conjugated primary antibody was used in the pulse-labeling step instead, the difference between control and AAS-treated cells remained, presumably because flow cytometry detected both surface and internalized fluorescent primary antibodies (Fig 2D). Next, we performed qPCR in NIH-3T3 and HepG2 cells. In both cells, the effects of AAS on LDLR mRNA expression appeared to be variable; nevertheless, the differences were not statistically significant (Fig 2E). Consistently, western blotting experiments showed no significant changes in total LDLR protein levels in AAS-treated cells (Fig 2F). Moreover, we provided evidence showing that pretreatment with actinomycin D (to block mRNA synthesis) or cycloheximide (to block protein synthesis) did not influence AAS-stimulated LDL endocytosis (Fig 2G). These data together indicated that, at least in the acute phase (within 2 h), AAS-induced increases in the cell surface LDLR availability and lipoprotein uptake did not require *de novo* LDLR gene expression.

AAS regulates LDLR recycling

To understand how AAS increased the amount of LDLRs on the cell surface, we characterized changes in the localization of LDLR in various endosomal trafficking compartments. In unstimulated cells, the majority of LDLRs were located in the perinuclear region, as shown by both immunofluorescence and ectopic expression of GFP-LDLR (Fig 3A). These perinuclear LDLRs mostly showed co-localization with Rab11 and Rab4a (Fig 3B and Appendix Fig S6A), indicating that the majority of intracellular LDLRs resided in the RE compartment under homeostatic condition. AAS treatment increased the amount of LDLRs residing in vesicular structures away from the perinuclear center (Fig 3C and Appendix Fig S6B). Further experiments using ectopic GFP-tagged proteins combining with immunolabeling revealed that, in the cytosolic space away from the perinuclear RE center, AAS increased LDLR co-localization with EEA1, Rab4a, and Rab5 (Fig 3D and Appendix Fig S6C, and Appendix Table S1). To exclude possible interferences with intracellular protein localization induced by ectopic overexpression, we confirmed these findings in separate tests by double labeling of endogenous proteins only (Appendix Fig S6D). In contrast, LDLRs displayed little co-localization with Rab7 (marker of late endosome) or Vps35 (marker of retromer), either without or with AAS treatment (Fig 3D and Appendix Fig S6C, and Appendix Table S1). Especially, LDLRs showed a high degree of co-localization with Rab4a, and AAS increased the abundance of Rab4a-associated LDLRs in the cell periphery (Fig 3E). These data indicated that AAS probably increased the amount of LDLRs in the fast recycling EE system. However, it should be noted that the size of the intracellular LDLR pool in each single cell is variable; therefore, the fluorescence intensity and/or area are not directly comparable on a cell-to-cell basis.

To directly demonstrate the increased rate of LDLR recycling, we performed surface biotin-disulfide pulse-chase labeling experiments as described (Gu *et al*, 2010), and demonstrated that the rate of clearance of internalized biotin-LDLRs (from the peak of curves) was accelerated in AAS-treated cells (Fig 3F). However, it is also observed that the peak of intracellular biotin-LDLR signal was shifted to the left in AAS-treated cells, presumably reflecting the accelerated endocytic process. Because there was evidence suggesting that an enhanced activity of the Rab4-dependent fast recycling pathway could substantially influence the endocytic recycling rate of membrane receptors (Arjonen *et al*, 2012), we next examined in more detail the relationship between AAS-induced LDLR trafficking and Rab4a. Overexpression of the dominant negative Rab4a-S22N suppressed the effect of AAS on LDL endocytosis, while the constitutively active Rab4a-Q67L enhanced LDL endocytosis in both resting and AAS-stimulated cells (Fig 3G). Although overexpression of WT Rab4a had no significant effect on LDL uptake in resting cells, but it enhanced the response induced by AAS (Fig 3G). In addition, we performed double labeling experiments, which confirmed that Rab4a-Q67L exhibited co-localizations with LDLRs in both of the perinuclear region and cell periphery, whereas Rab4a-S22N only co-localized with LDLRs in the perinuclear region (Fig 3H and Appendix Fig S6E, and Appendix Table S1). These data raise the possibility that AAS may accelerate LDLR trafficking by expanding the capacity of the Rab4-sensitive fast recycling route. To examine whether AAS could similarly increase the trafficking of other cargo receptors, we analyzed intracellular distribution of TfRs. It was

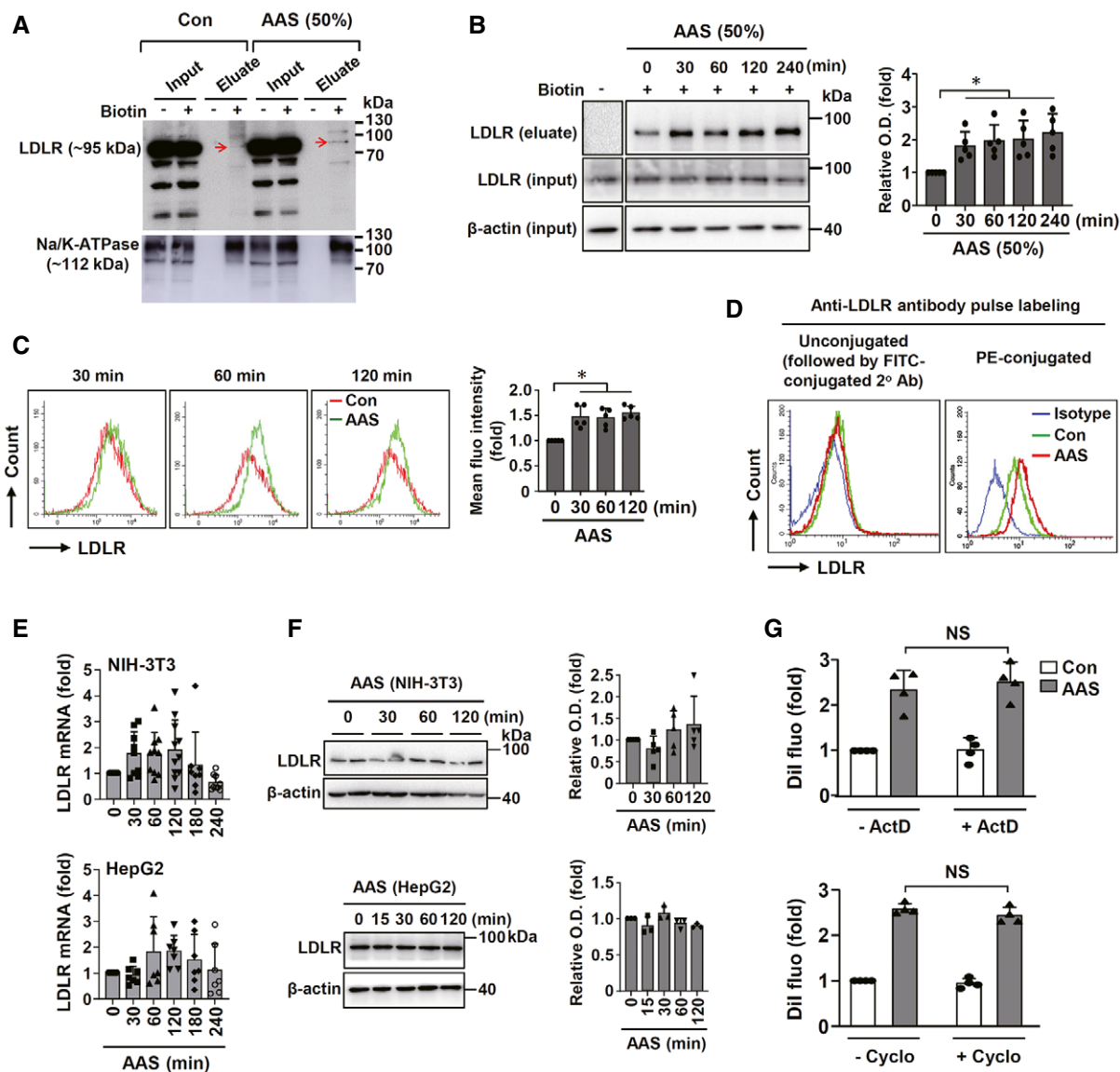


Figure 2. AAS increased the amount of LDLRs on the cell surface independent of *de novo* gene expression.

- A** Preliminary western blot analysis of samples from the cell surface protein biotinylation and pull-down assay (example from 2 independent experiments with similar results) showing that only a minor fraction of LDLRs (red arrows) were located on the surface of plasma membrane (eluate). Na-K ATPase was used as a membrane marker. Samples omitting the biotinylation step (Biotin –) were included as negative control. Experiments were performed in NIH-3T3 cells.
- B** Western blots and quantitative densitometry data showing that AAS increased the amount of LDLRs on plasma membrane. The eluate samples obtained as indicated in panel A were further concentrated before western blotting.
- C** Flow cytometry with nonpermeabilized NIH-3T3 cells showing that AAS increased the abundance of LDLRs on the cell surface. The quantitative data were shown on the right.
- D** Anti-LDLR antibody pulse labeling followed by flow cytometry showing that the detected PM surface LDLRs in both resting and AAS-treated cells participated in the endocytic turnover. In the left panel, the cells were pulse-labeled with unconjugated LDLR antibody at 4°C, then returned to 37°C for 60 min, and finally labeled with FITC-conjugated secondary antibody (2° Ab) at 4°C. In the right panel, the cells were pulse-labeled with PE-conjugated primary antibody using the same protocol, and flow cytometry was carried out without secondary antibody labeling. Isotype Ig was used as negative control. Data shown were example from 3 independent experiments with similar results.
- E** Real-time PCR results showing that AAS had no significant effects on LDLR mRNA levels in NIH-3T3 and HepG2 cells.
- F** Western blots and quantitative densitometry data showing that AAS had no significant effects on the total LDLR protein levels.
- G** Fluorescence microscopy data showing that pretreatment with actinomycin D (ActD, 10 μ g/ml) or cycloheximide (Cyclo, 30 μ g/ml) in NIH-3T3 cells did not change AAS (50%)-stimulated DiI-LDL endocytosis.

Data information: Data were mean \pm SD. * P < 0.05, one-way ANOVA. NS, no significance.

Source data are available online for this figure.

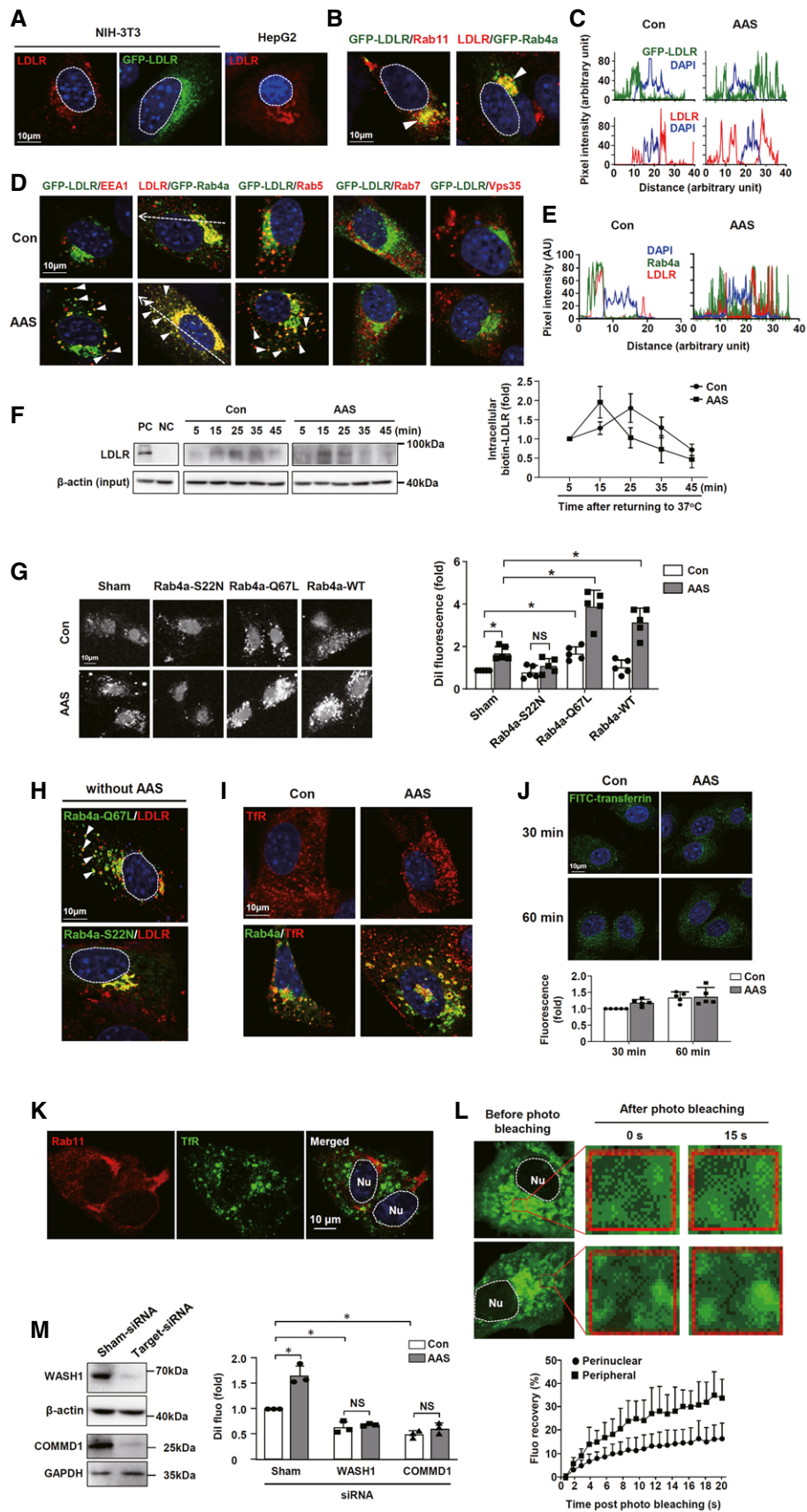


Figure 3.

Figure 3. Effects of AAS on LDLR recycling.

- A Intracellular distribution of LDLRs revealed by immunofluorescence staining (red) or ectopic expression of GFP-LDLR (green) in unstimulated NIH-3T3 and HepG2 cells. Cell nuclei were counterstained with DAPI (outlined by the dotted lines).
- B Double fluorescence labeling assays illustrating that LDLRs exhibited partial co-localization with Rab11 and Rab4a in the perinuclear region (indicated by arrowheads) in unstimulated cells.
- C Results of fluorescence intensity profile analysis (original images shown in Appendix Fig S6B) showing that AAS (50%) treatment induced a redistribution of LDLRs toward the cell periphery in NIH-3T3 cells. Note the increased red/green signals distal to the nuclei (DAPI). Con, complete culture medium.
- D Double fluorescence labeling assays illustrating that AAS increased LDLR co-localization with EEA1, Rab4a, and Rab5 (mainly in the peripheral region) (arrowheads), whereas LDLRs displayed little co-localization with Rab7 or Vps35 either without or with AAS treatment.
- E Fluorescence intensity profile analysis (sampling locations as indicated by the dotted lines in panel D) showing that AAS increased LDLR co-localization with Rab4a in the cell periphery.
- F Results of surface biotin-disulfide pulse-chase labeling experiments showing that AAS accelerated the mobilization of LDLRs for both of the entry into and the exit from the intracellular space (mean data from 3 independent experiments). PC, positive control (sample omitting the disulfide cleavage step); NC, negative control (sample omitting the biotinylation step).
- G Fluorescence microscopy data showing that overexpressing dominant negative Rab4a-S22N suppressed AAS-stimulated Dil-LDL endocytosis, whereas overexpressing constitutively active Rab4a-Q67L mimicked the effect of AAS in resting cells. Overexpressing WT Rab4a enhanced AAS-induced response but had no effect in unstimulated cells.
- H Double fluorescence labeling experiments showing that, in unstimulated cells, Rab4a-Q67L exhibited co-localization with LDLRs in both of the perinuclear region and the cell periphery (arrowheads), whereas Rab4a-S22N only co-localized with LDLRs in the perinuclear region.
- I Double immunofluorescence labeling showing that there was not a perinuclear pool for transferrin receptor (TfR) in unstimulated cells. Although TfRs also showed co-localization with Rab4a throughout the cytosol, this pattern of distribution was not affected by AAS treatment.
- J Fluorescence microscopy data showing that AAS did not increase the rate of endocytosis of FITC-labeled transferrin.
- K Representative double fluorescence labeling results illustrating that there was not a significant perinuclear co-localization between Rab11 and TfR in unstimulated cells.
- L FRAP assay results in the cells expressing GFP-LDLR showing that fluorescence recovery in the putative perinuclear pool was slower than that in the peripheral region. The quantitative data shown below were average values from 8–10 individual cells.
- M Inhibitory effects of gene silencing for WASH1 and COMMD1 on the basal and AAS-stimulated LDL uptake. Left panels, representative western blots showing gene silencing efficacy of the siRNA constructs (from 3 independent experiments with similar results). Right panel, quantitative Dil fluorescence microscopy data showing that WASH1 and COMMD1 gene silencing reduced the basal level of LDL uptake and also abolished the response induced by AAS.

Data information: Data were mean \pm SD. * $P < 0.05$, one-way ANOVA. NS, no significance. All immunofluorescence labeling experiments were repeated at least three times. Experiments in (B) to (J) were performed in NIH-3T3 cells; (K) to (M) in HepG2 cells. Nu, nucleus.

Source data are available online for this figure.

found that there was not a perinuclear pool of TfRs in unstimulated cells, which was in contrast to LDLRs (Fig 3I). Although TfRs also showed co-localization with Rab4a throughout the cytosol, this pattern of distribution was not affected by AAS treatment (Fig 3I and Appendix Fig S6F, and Appendix Table S1). Consistently, AAS did not increase the rate of endocytosis of FITC-labeled transferrin (Fig 3J). These data suggest that the increased amount of LDLRs in the fast recycling compartment in AAS-treated cells is dependent on the presence of a perinuclear pool of the receptors, which presumably might serve as an intracellular reservoir. To further strengthen this argument, we performed more double labeling experiments, which showed that there was not a significant perinuclear Rab11-TfR co-localization (Fig 3K). To distinguish that the perinuclearly and peripherally localized LDLR populations had different trafficking dynamics, we performed FRAP assays in AAS-treated cells. As shown in Fig 3L, the rate of LDLR fluorescence recovery in the perinuclear region was slower than that in the peripheral region, indicating the slow recycling nature of the perinuclear LDLR pool as compared to the peripheral LDLR population. Taken together, these data suggest that, under the present experimental settings, the majority of Rab4-associated-TfRs are located in the fast recycling compartment regardless of AAS treatment, while the presence or absence of the putative perinuclear (slow recycling) receptor pool may explain the difference in AAS responsiveness between LDLR versus TfR.

In order to confirm the effects of Rab4a-S22N overexpression, we also did gene silencing for endogenous Rab4a (Appendix Fig S7A), and demonstrated that Rab4a depletion diminished the responsiveness

of AAS-induced LDL endocytosis (Appendix Fig S7B). To further validate the finding that AAS stimulated LDLR translocation to the plasma membrane, we adapted our immuno-labeling protocol by using nonpermeabilized cells with an avidin-biotin complex strategy, which allowed us to successfully detect membrane located LDLRs with confocal microscopy. We showed that AAS significantly increased the abundance of LDLRs on the plasma membrane (Appendix Fig S8). However, a limitation of this study was that direct measurement of the amount of GFP-tagged LDLRs on the cell surface was not performed. Moreover, in order to clarify whether the LDL uptake stimulated by AAS depended on the conventional LDLR sorting/recycling machinery, we performed gene silencing for WASH1 (WASH complex subunit 1) and COMMD1 (Bartuzi *et al*, 2016). It was demonstrated that depletion of these components not only reduced the basal level of LDL uptake but also abolished the response induced by AAS (Fig 3M), indicating that AAS-stimulated LDL uptake did not require a distinct sorting/recycling pathway.

AAS-stimulated LDL endocytosis was dependent on Ca^{2+} and CaMKII signaling

To understand the signaling mechanisms of AAS-induced response, we performed gene silencing for GCN2 (Appendix Fig S9), a known effector kinase activated by AAS (Castilho *et al*, 2014). However, knocking down GCN2 expression did not modify AAS-stimulated LDL endocytosis (Fig 4A). To confirm these data, we also pretreated the cells with GCN2iB, a potent ATP-competitive inhibitor of GCN2, and demonstrated that GCN2iB had no effect on AAS-stimulated

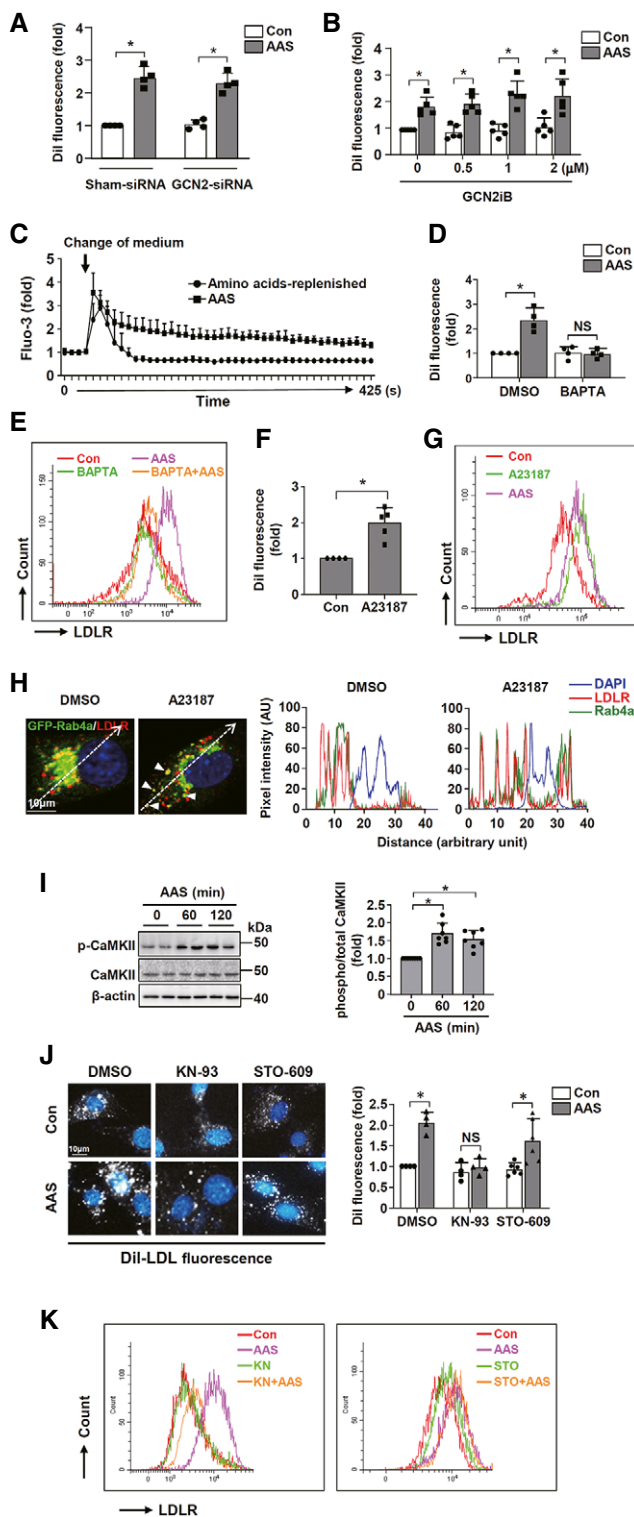


Figure 4. AAS-stimulated LDL endocytosis was dependent on Ca^{2+} and CaMKII signaling.

- A** Fluorescence microscopy data showing that knocking down GCN2 expression with siRNA did not modify AAS-stimulated DiI-LDL endocytosis.
- B** Fluorescence microscopy data showing that pretreatment of the cells with the GCN2 inhibitor GCN2iB had no effect on AAS-stimulated DiI-LDL endocytosis.
- C** Measurement of intracellular Ca^{2+} concentration using fluorescent confocal microscopy in living cells incubated in AAS medium and medium with amino acids replenished, respectively (mean data of $n = 3$ independent experiments).
- D** Fluorescence microscopy data showing that pretreating cells with the Ca^{2+} chelator BAPTA-AM (5 μ M) abolished the effect of AAS on DiI-LDL endocytosis. DMSO was vehicle control.
- E** Flow cytometry analysis showing that BAPTA-AM pretreatment abolished AAS-induced increase in the cell surface LDLRs (example from 3 independent experiments with similar results).
- F** Fluorescence microscopy data showing that treatment with the calcium ionophore A23187 (2 μ M for 120 min) enhanced DiI-LDL endocytosis in the cells maintained in complete medium.
- G** Flow cytometry analysis showing that A23187 produced a comparable effect as AAS on the abundance of the cell surface LDLRs in the cells maintained in complete medium (experiment repeated 3 times).
- H** Double fluorescence labeling and fluorescence intensity profile analysis showing that A23187 increased LDLR-Rab4a co-localization in the cell periphery (arrowheads) (example from 3 independent experiments with similar results). Dotted lines indicated the sampling location for fluorescence intensity profile analysis. DMSO was vehicle control.
- I** Western blots and densitometry data showing that AAS increased the level of CaMKII phosphorylation (Thr286).
- J** Fluorescence microscopy images and quantitative data showing that pretreatment with the CaMKII inhibitor KN-93 (5 μ M), but not the calcium/calmodulin-dependent kinase kinase inhibitor STO-609 (5 μ M), abolished AAS-stimulated DiI-LDL endocytosis.
- K** Flow cytometry data showing that KN-93, but not STO-609, abolished AAS-stimulated increase in the cell surface LDLR abundance (experiment repeated 3 times). Experiments in A were performed in HepG2 cells; other experiments were in NIH-3T3 cells.

Data information: Data were mean \pm SD. * $P < 0.05$, one-way ANOVA or unpaired t-test as appropriate. NS, no significance. Source data are available online for this figure.

LDL endocytosis (Fig 4B). Given the acute nature of AAS-induced response, we tested whether it was related to Ca^{2+} signaling as inspired by observations from other researchers (Ghislat *et al*, 2012). Using intracellular calcium imaging, we showed that AAS induced a quick elevation in intracellular Ca^{2+} concentration

(Fig 4C). Pretreating cells with the membrane permeable Ca^{2+} chelator BAPTA-AM abolished the effect of AAS on LDL endocytosis (Fig 4D and Appendix Fig S10). BAPTA-AM also abolished AAS-induced increase in the abundance of the cell surface LDLRs (Fig 4E). Conversely, we demonstrated that the treatment with the calcium ionophore A23187 mimicked the effects of AAS on LDL endocytosis (Fig 4F and Appendix Fig S11), the cell surface availability of LDLRs (Fig 4G), and LDLR-Rab4a co-localization in the cell periphery (Fig 4H and Appendix Table S1). To determine whether CaMKII could be involved in mediating AAS-induced effects, we measured CaMKII auto-phosphorylation by western blotting, revealing that AAS stimulation augmented CaMKII (Thr286) phosphorylation (Fig 4I). Functionally, inhibition of CaMKII with the selective inhibitor KN-93 abolished AAS-stimulated LDL endocytosis and mobilization of LDLRs to the cell surface (Fig 4J and K), while KN-93 alone had no effects. In comparison, pretreatment with STO-609, an inhibitor of calcium/calmodulin-dependent kinase (the upstream activator of CaMKII/IV), did not change AAS-induced effects (Fig 4J and K).

CaMKII regulates Rab4a functions

Next, we investigated the possible mechanism by which CaMKII mediated AAS-induced effects. There is evidence suggesting that increased interaction between Rab4 and its guanosine nucleotide dissociation inhibitor (GDI) facilitates Rab4-mediated receptor recycling to the synaptic membrane in neurons, and this is mediated by phosphorylation of GDI on Ser213 (Liu *et al*, 2010). Hence, we examined the binding between Rab4a and GDI after AAS treatment. However, using immunoprecipitation and double fluorescence labeling, we did not detect a change in Rab4a-GDI binding in AAS-treated cells (Fig 5A and B). Then we asked whether CaMKII could directly affect Rab4 functions by phosphorylation. By analyzing the amino acid sequence of Rab4a, we identified a putative CaMKII substrate motif (R-X-X-S*/T*) (White *et al*, 1998) at Thr137, and this motif was conserved across different species (Fig 5C). Next, we performed *in vitro* phosphorylation experiments with wild type and the corresponding 137T-to-A mutant of Rab4a(120-154), and showed that CaMKII could phosphorylate the wild-type peptide, but failed to phosphorylate the mutant substrate (Fig 5D). To further corroborate this finding, we overexpressed full-length wild-type Rab4a and Rab4a-T137A mutant in NIH-3T3 cells. It was shown that AAS increased the phosphorylation level of wild-type Rab4a, but not Rab4a-T137A (Fig 5E and Appendix Fig S12A). Moreover, we confirmed that AAS also increased the phosphorylation level of endogenous Rab4a in NIH-3T3 cells; this response was abolished by the CaMKII inhibitor KN-93 (Fig 5F and Appendix Fig S12B). To test the functional importance of Rab4a phosphorylation in LDL endocytosis, we overexpressed Rab4a-T137A, and found that in cells with a high level of Rab4a-T137A expression, AAS failed to stimulate LDL endocytosis (Fig 5G and Appendix Fig S13). In comparison, we observed that cells with poor expression of the ectopic Rab4a-T137A retained the responsiveness to AAS (Fig 5G and Appendix Fig S13). We also confirmed that Rab4a-T137A overexpression blunted the effect of AAS on LDLR mobilization to PM

using surface biotinylation assay (Fig 5H and Appendix Fig S12C). To further establish the role of phosphorylation events in mediating AAS-induced LDL endocytosis, we treated the cells with okadaic acid, a serine/threonine protein phosphatase inhibitor, which significantly increased the phosphorylation level of CaMKII (Fig 5I). We showed that okadaic acid treatment mimicked the effects of AAS on LDL endocytosis and LDLR-Rab4a co-localization in the periphery of intracellular space in nonstarved cells (Fig 5J and K, and Appendix Table S1). Because there is evidence showing that Rabenosyn-5, an effector protein binding to both Rab4 and Rab5, has a critical role in facilitating the fast recycling of TfR from EE (de Renzis *et al*, 2002), hence we examined whether CaMKII-mediated Rab4 phosphorylation affected Rab4 binding with Rabenosyn-5. We demonstrated that AAS increased the binding between wild-type Rab4a and Rabenosyn-5, and this response was abolished in the presence of KN-93 (Fig 5L and Appendix Fig S12D). On the other hand, the binding between Rabenosyn-5 and Rab4a-T137A was relatively weak, and was not affected by AAS (Fig 5L and Appendix Fig S12D).

AAS-induced increase in LDL uptake is comparable to that induced by statin

In the preliminary test, we found that treatment of NIH-3T3 cells with pravastatin at 50 μ M upregulated the expression of LDLR as early as 4 h (Fig EV2A). Using the 4-h time point, we showed that pravastatin but not AAS significantly increased the mRNA and protein levels of LDLR (Fig EV2B). In comparison, both AAS and pravastatin produced comparable stimulatory effects on LDL uptake in NIH-3T3 and HepG2 cells (Fig EV2C). We thought that the quick response of LDLR expression to pravastatin might be related to the relatively high concentration of pravastatin used; thus we tested the effect of pravastatin at 5 μ M. We showed that pravastatin at low and high concentrations clearly exhibited different time courses of LDLR induction (Fig EV2D). Furthermore, we confirmed that 5 μ M

Figure 5. CaMKII phosphorylated Rab4a and regulated its functions in NIH-3T3 cells.

- A Immunoprecipitation (IP) and western blot (WB) experiments in cells expressing GFP-Rab4a fusion protein showing that AAS did not change the interaction between Rab4a and GDI. H/chain, Ig heavy chain. Normal IgG was used as negative control for IP.
- B Double fluorescence labeling experiment showing that AAS had no effect on Rab4a-GDI co-localization (experiment repeated 3 times).
- C Sequence alignment of the putative CaMKII substrate site (Thr137) in Rab4a across different species.
- D *In vitro* phosphorylation experiments using FLAG-tagged wild type (WT) and T137A mutant of Rab4a(120-154) peptide showing that CaMKII could phosphorylate the wild-type peptide (experiment repeated 2 times). p-(S/T), anti-phospho serine/threonine antibody.
- E Representative results of IP/WB experiments in NIH-3T3 cells expressing wild-type GFP-Rab4a or GFP-Rab4a-T137A, showing that AAS increased the phosphorylation of wild-type Rab4a but not Rab4a-T137A.
- F Representative results of IP/WB experiments showing that AAS increased the phosphorylation level of endogenous Rab4a, and this response was abolished by KN-93 pretreatment.
- G Representative fluorescence microscopy images showing that in the cells with a high level of Rab4a-T137A expression (arrows), AAS failed to stimulate DiI-LDL endocytosis, while in cells with poor Rab4a-T137A expression (asterisk), AAS-stimulated DiI-LDL endocytosis was retained.
- H Surface protein biotinylation assay showing that Rab4a-T137A overexpression diminished the effect of AAS on LDLR accumulation on PM (example from 3 independent experiments with similar results).
- I Western blots and quantitative data showing that treatment with the serine/threonine protein phosphatase inhibitor okadaic acid (OA, 0.5 μ M for 60 min) increased the phosphorylation level of CaMKII (Thr286) in nonstressed cells.
- J Fluorescence microscopy data showing that okadaic acid treatment in nonstressed cells mimicked the effect of AAS on DiI-LDL endocytosis.
- K Double fluorescence labeling and fluorescence intensity profile analysis showing that okadaic acid treatment in nonstressed cells increased LDLR-Rab4a co-localization in the cell periphery (arrowheads) (experiment repeated 3 times). Dotted lines indicated the sampling location for fluorescence intensity profile analysis.
- L Representative IP/WB results showing that in cells overexpressing GFP-Rab4a fusion proteins, AAS increased Rabenosyn-5 binding with wild-type Rab4a, but not that with Rab4a-T137A. The stimulating effect of AAS on Rabenosyn-5/Rab4a binding was blunted in the presence of KN-93.

Data information: Data were mean \pm SD. * P < 0.05, one-way ANOVA or unpaired t -test as appropriate. Source data are available online for this figure.

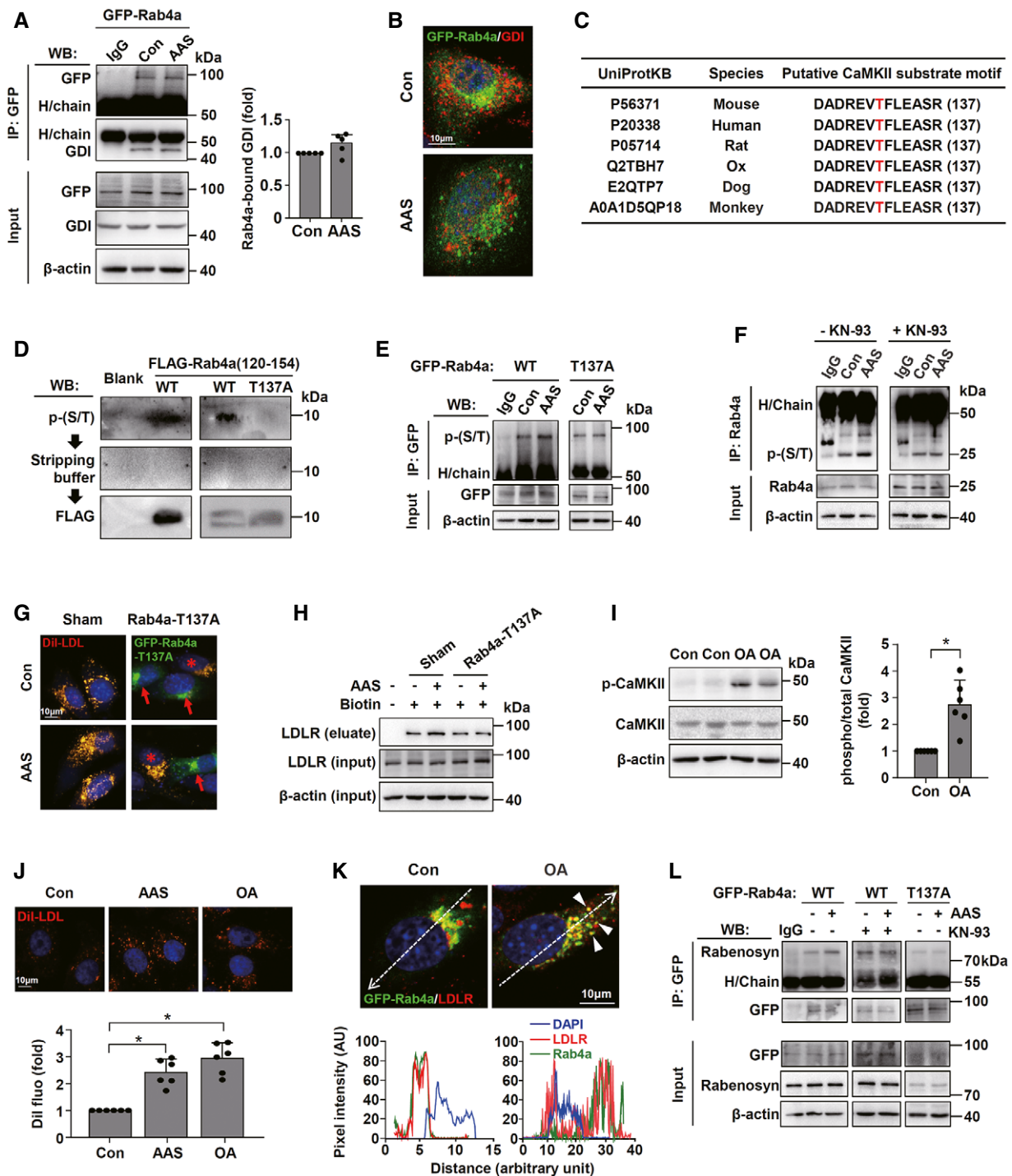


Figure 5.

pravastatin with a prolonged treatment duration (12 h) similarly enhanced LDL endocytosis (Fig EV2E).

Effects of *in vivo* dietary amino acid interventions on LDL clearance

To understand the physiological relevance of AAS-stimulated cellular LDL uptake *in vivo*, we first tested the effect of acute dietary

AAS challenge in wild-type mice. It was demonstrated that dietary AAS for up to 72 h increased the rate of LDL uptake by the liver (Fig 6A–C). This effect was not associated with changes in the expression of LDLRs in the liver (Fig 6D). To further validate the Dil fluorescence data in liver tissues, we performed western blot experiments using an antibody against human ApoB as a measure of LDL internalization, as the infused LDL preparation was of human origin. We confirmed that this antibody is not reactive to the

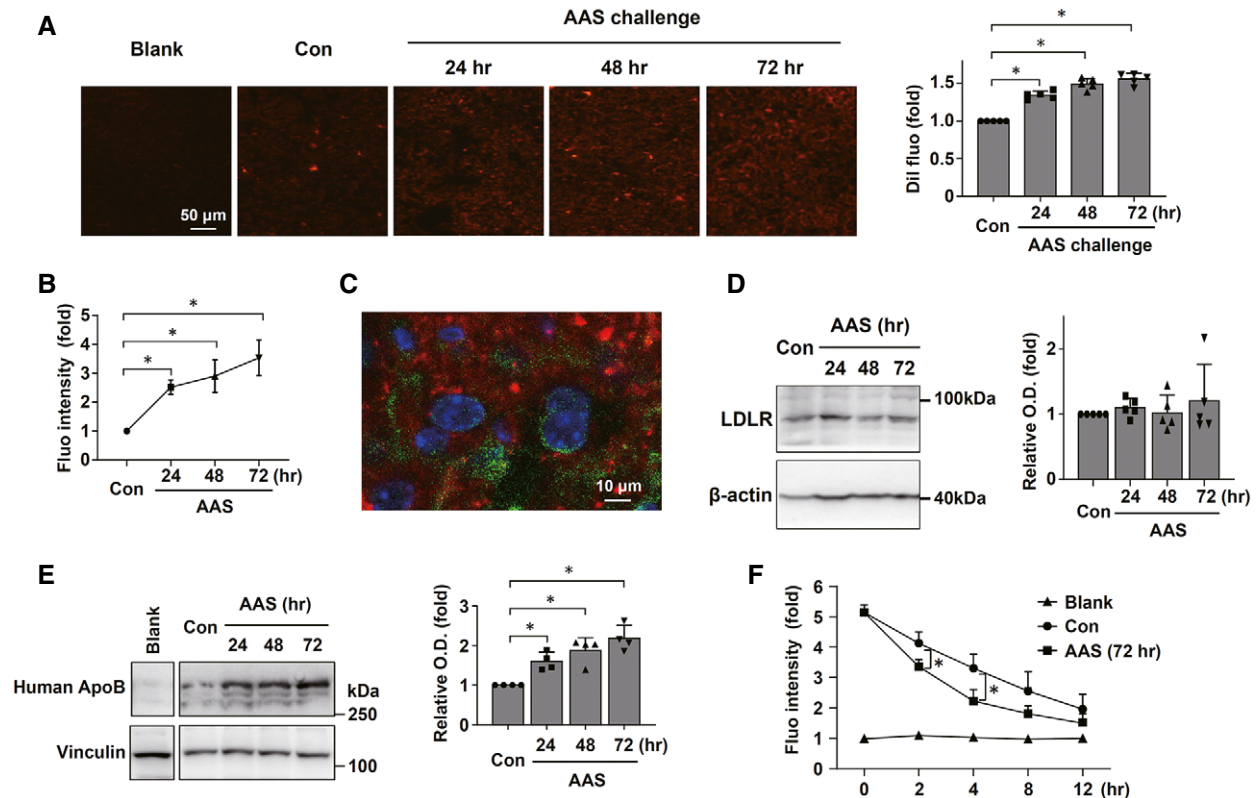


Figure 6. Effects of acute dietary AAS intervention on LDL clearance *in vivo*.

- A Fluorescence microscopic images of liver sections from wild-type mice and corresponding quantitative data showing that dietary AAS for up to 72 h acutely increased the rate of DiI-LDL (red fluorescence) uptake by hepatocytes.
- B DiI fluorescence intensity measured in the supernatants of liver tissue homogenates from wild-type mice without and with AAS treatment, using microplate reader (data normalized to tissue weight).
- C A representative fluorescence microscopic image showing the intracellular localization of the DiI signal (red fluorescence) in hepatocytes following intravenous DiI-LDL infusion (preliminary data from animal with 72-h dietary AAS). The cell membrane was labeled with Alexa Fluor-488 conjugated wheat germ agglutinin (green); the nucleus was stained with DAPI (blue).
- D Representative western blots and densitometry data showing that dietary AAS for up to 72 h did not change the expression level of LDLRs in the liver.
- E Western blot images and quantitative densitometry data showing that accumulation of human ApoB protein in the liver was increased in AAS-challenged mice following intravenous infusion of human LDL preparations.
- F Spectrofluorometry data obtained in plasma samples showing that the rate of DiI-LDL clearance from the systemic circulation was increased in AAS-challenged animals.

Data information: (A), (B), (C), and (E) were performed 2 h after LDL infusion. Blank samples were from animals infused with saline. Data were mean \pm SD. * $P < 0.05$, one-way ANOVA ($n = 3$ for panel (B); $n = 4$ for panel (F), independent experiments). Source data are available online for this figure.

endogenous murine ApoB (Fig 6E). We showed that in AAS-challenged animals, the accumulation of human ApoB in the liver was significantly enhanced (Fig 6E). In addition, we directly measured the clearance of DiI-LDL in the plasma using spectrofluorometry; we demonstrated that the rate of DiI-LDL clearance from the systemic circulation was increased in AAS-challenged animals (Fig 6F). In order to verify that the observed *in vitro* cellular effects of AAS were preserved under *in vivo* conditions, we repeated several key assays in the liver tissue. In contrast to the results shown in Fig 6D, we demonstrated that acute AAS treatment significantly increased the amount of LDLRs on the plasma membrane fraction (Fig EV3A). Furthermore, we showed that AAS treatment *in vivo* enhanced Rab4a phosphorylation and Rab4a/Rabenosyn-5 interaction in the liver (Fig EV3B).

Next, we asked whether dietary amino acid intervention would have beneficial effects on systemic LDL metabolism under hypercholesterolemia condition. A technical difficulty for this purpose is that it is impossible to perform total dietary amino acid deprivation *in vivo* for a long term; therefore, we adopted a strategy of reducing the dietary amino acid content by 50% as inspired by some recent studies (Maida *et al*, 2018; Yap *et al*, 2020). This intervention did not cause obvious adverse effects in the animals. In heterozygous *LDLR*^{+/-} mice, feeding a HF diet for 2 to 4 weeks increased the serum LDL cholesterol and total cholesterol levels. Concomitant reduction in dietary amino acid supply without enforced calorie restriction ameliorated HF-induced hypercholesterolemia (Fig EV4A). Further FPLC analysis revealed that the levels of both LDL and VLDL fractions were reduced in response to dietary amino

acid restriction, whereas the HDL level was not changed (Fig EV4B). Interestingly, these data demonstrated that the HF diet used in this study mainly increased VLDL/LDL levels but not that of HDL in *LDLR*^{+/-} mice; this pattern of change was in line with the observation that dieting only ameliorated HF-induced hypercholesterolemia, but did not further decrease the basal level of blood cholesterol (which was predominantly determined by HDL in mice). It was argued that this *in vivo* dietary strategy was not in contradiction to our *in vitro* findings, since we demonstrated that the enhanced cellular LDL uptake did not require complete amino acid removal, while 50% reduction of amino acids alike had significant effects.

LDL endocytosis compensates for autophagy induction under AAS condition in cells

Using western blotting, qPCR, and immunofluorescence, we showed that AAS elicited autophagic response from 2 to 4 h in HepG2 cells, while addition of exogenous LDL blunted the response (Fig 7A–C). We verified that the AAS-induced increase in LC3-II was not accompanied by accumulation of p62/SQSTM1 (Appendix Fig S14), indicating that the effect of AAS under current experimental settings was not due to blockade of the normal autophagic flux. The difference of the time-course of AAS-induced autophagy in comparison to the data in Appendix Fig S3 was due to the fact that these experiments were carried out under a serum-free condition. Next, we showed that the retarding effect of exogenous LDL on autophagy was lost in *LDLR*^{-/-} hepatocytes as compared to WT cells (Fig 7D). Moreover, pretreatment with KN-93 or Pitstop2 abolished the compensatory effect of LDL (Fig 7E). In NIH-3T3 cells, we confirmed the similar compensatory effect of LDL on autophagy induction, and further demonstrated that the effect of LDL was attenuated by overexpression of Rab4a-T137A (Fig 7F). To conclusively show that lysosomal LDL catabolism was crucial for the suppressive effect of LDL on AAS-induced autophagy, we tested different lysosome inhibitors, including the v-ATPase inhibitors bafilomycin A1 and concanamycin A, and the lysosomal protease inhibitor leupeptin. We found that bafilomycin A1 and concanamycin A both potently inhibited the basal LDL endocytic activity (Fig EV5A), making these compounds unsuitable for this experimentation. In comparison, leupeptin up to 10 μ M showed no effect on basal endocytosis (Fig EV5A). Using LysoTracker staining, we next confirmed that, unlike the v-ATPase inhibitors, leupeptin had no effect on lysosome acidification (Fig EV5B). Then we tested the effect of leupeptin on the basal autophagic activity in resting cells. As shown in Fig EV5C, we found that leupeptin moderately increased the basal level of autophagy, with a slight increase in p62/SQSTM1. It was likely that the increase in p62/SQSTM1 following leupeptin treatment was due to compromised lysosomal degradation, rather than blockade of the autophagic flux. Finally, we demonstrated that the autophagy inhibiting effect of exogenous LDL was diminished by leupeptin pretreatment (Fig EV5D and E).

AAS does not increase the abundance of LRP1 or megalin/LRP2 on the cell surface

To clarify whether other cargo receptors than LDLR might be implicated in AAS-stimulated LDL uptake, we performed flow cytometry and confocal microscopy analyses for LRP1 and megalin/LRP2, two

LDLR related proteins which might be involved in clearance of cholesterol-rich (remnant) lipoproteins. However, these assays showed no evidence of increased translocation of LRP1 or megalin/LRP2 to the cell surface in response to AAS (Appendix Fig S15A and B), strongly supporting that AAS-induced cargo receptor trafficking is a receptor type-specific phenomenon.

Discussion

Here, we report a novel mechanism which may increase the cell surface LDLR availability without changing the homeostasis of LDLR mRNA or protein, in comparison to the actions of statins and PCSK9 inhibitors. Specifically, reducing the supply of free amino acids triggers deployment of intracellular LDLRs (likely from a perinuclear compartment) to the PM, thereby increasing the rate of LDL endocytosis. This response is independent of the induction of autophagy. Conversely, our data indicate that AAS-induced LDL endocytosis may represent an alternative nutrient stress response which counterbalances autophagy induction in the presence of usable extracellular nutrient sources (such as lipoproteins). At the cellular level, the stimulatory effect of AAS on LDL uptake is comparable to that induced by pravastatin. It is thought that such an alternative pathway may help to prevent potential disadvantages caused by exaggerated autophagic response under amino acid stress. At the systemic level, as indicated by the *in vivo* data, this response may facilitate LDLR-dependent tissue uptake of apolipoprotein B-containing LDL/VLDL particles, thereby increasing the clearance of these atherogenic lipoprotein molecules from the circulation.

Indeed, the mechanisms by which the cells regulate LDLR recycling remain largely enigmatic (van Wijers *et al*, 2015; de Sluis *et al*, 2017; Vos *et al*, 2018). Apart from several Rab proteins, the CCC (COMMD/CCDC22/CCDC93) and WASH (Wiskott–Aldrich Syndrome Protein and SCAR Homolog) complexes have been found to be critical in sorting LDLRs into the recycling route, but not for lysosomal degradation (Bartuzi *et al*, 2016). In addition, sorting nexin 17 (SNX17) appears to be another constitutive component at the sorting interface in EEs, directing LDLRs back to PM (Burden *et al*, 2004). Our study points to an essential role of the Rab4a-dependent fast recycling route in AAS-stimulated LDL endocytic. We propose that AAS, via Ca^{2+} /CaMKII-mediated Rab4a phosphorylation, expands the volume of the LDLR fast recycling compartment, leading to increased presentation of LDLRs on the PM (see Fig 8). However, our data in Fig 3G suggest that GTP loading on Rab4 is a prerequisite for CaMKII-mediated phosphorylation to take effect, because overexpression of the GDP-locked mutant Rab4a-S22N blunts the effect of AAS on LDL endocytosis, whereas the GTP-locked Rab4a-Q67L not only mimics the effect of AAS in resting cells, but also enhances the stimulating effect of AAS.

Our data have also shown that CaMKII-mediated Rab4 phosphorylation increases the association between Rab4 and the effector protein Rabenosyn-5, and this change may explain the enhanced fast recycling of LDLR after AAS. This notion is highly supported by previous results showing that overexpression of Rabenosyn-5 increases the fraction of Rab4/Rab5-associated endosomal compartment and decreases the fraction of Rab4/Rab11-positive compartment, and this Rab4 redistribution is accompanied by a faster rate of

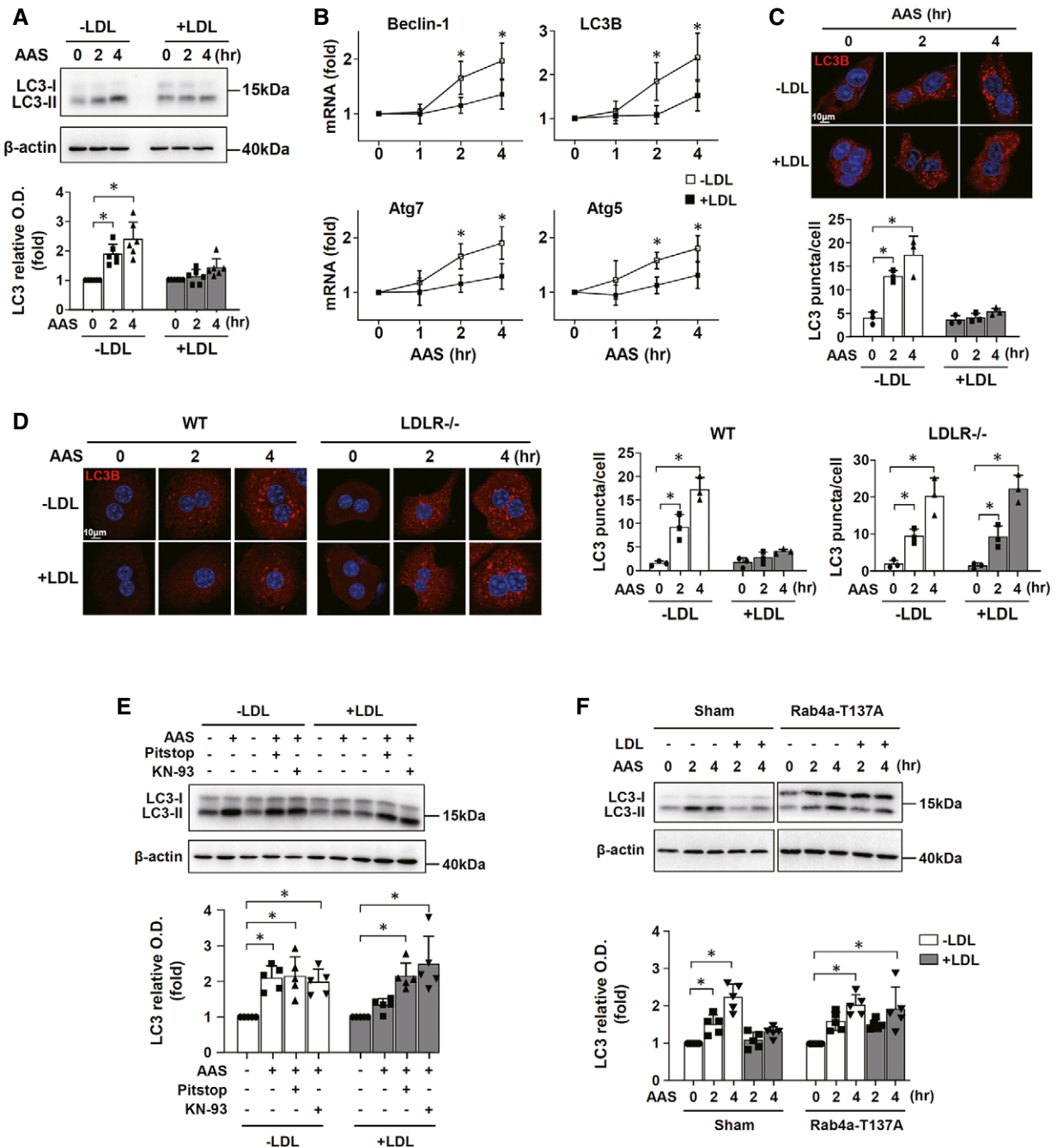


Figure 7. LDL endocytosis compensated for autophagy induction under AAS condition.

- A Western blots and quantitative densitometry data showing that AAS-induced autophagic response was delayed by addition of exogenous LDL (100 μ g/ml) in HepG2 cells.
- B Real-time PCR results showing that AAS-induced autophagic responses were delayed by exogenous LDL in HepG2 cells ($n = 4-5$ independent experiments).
- C Immunofluorescence data showing that exogenous LDL blunted AAS-induced LC3 puncta formation in HepG2 cells.
- D Immunofluorescence data showing that exogenous LDL blunted AAS-induced LC3 puncta formation in WT but not LDLR^{-/-} primary hepatocytes.
- E Western blot results showing that Pitstop2 (20 μ M) and KN-93 (5 μ M) abolished the compensatory effect of exogenous LDL on AAS-induced autophagic response in HepG2 cells.
- F Western blot results showing that in NIH-3T3 cells, the compensatory effect of exogenous LDL on autophagy induction in response to AAS was attenuated by overexpression of Rab4a-T137A.

Data information: Data were mean \pm SD. * $P < 0.05$, one-way ANOVA (except for the data in (E) and (F), which were examined with nonparametric Kruskal–Wallis test because of non-Gaussian distribution).

Source data are available online for this figure.

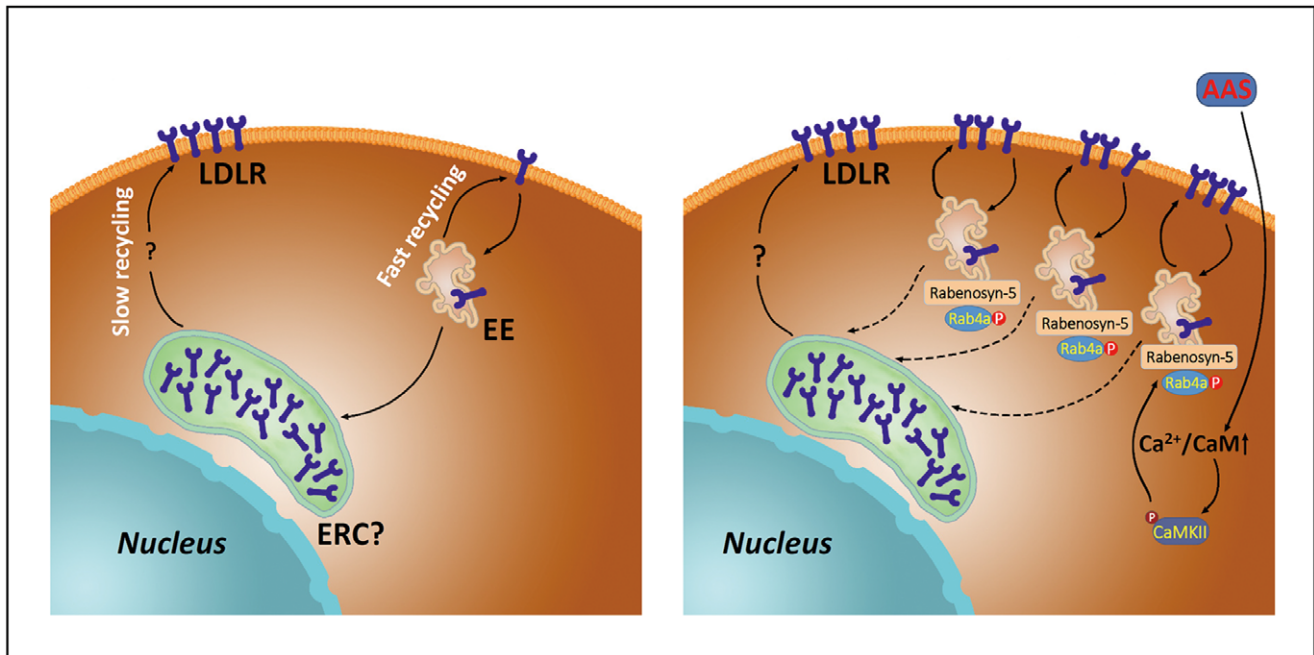


Figure 8. Summary of the potential mechanism by which amino acid starvation (AAS) increases LDL endocytosis.

In resting cells, an amount of LDLRs are stored in an intracellular (perinuclear) pool. Via Ca^{2+} /calmodulin (CaM) signaling and calcium/calmodulin-dependent protein kinase II (CaMKII)-mediated Rab4 phosphorylation, AAS increases the abundance of LDLRs residing in the fast recycling route, leading to increased availability of LDLRs on the cell surface. ERC, endocytic recycling compartment; EE, early endosome.

TfR recycling from early endosomes to the cell surface and reduced TfR transport to the perinuclear Rab11-containing endosomes (de Renzis *et al*, 2002). In this study, we have identified a conserved putative CaMKII substrate motif in Rab4a, which fulfills the optimal requirements for CaMKII preference, including an arginine at -3 , a hydrophobic residue at -5 (alanine), and a phenylalanine at $+1$ (Songyang *et al*, 1996; White *et al*, 1998). Our results are also consistent with previous reports that different serine/threonine kinases, including the mitogen-activated protein kinase ERK and the cyclin-dependent kinase CDK1, may mediate Rab4 phosphorylation thereby affecting the intracellular distribution of this protein (van der Sluijs *et al*, 1992; Cormont *et al*, 1994). However, the molecular basis for these phosphorylation-induced changes of Rab4 localization and function is not clearly understood.

Interestingly, our results indicate that AAS-induced deployment of intracellular LDLRs to the cell surface does not strictly require the presence of exogenous LDL, that is, the underlying endocytic recycling process may be constitutive or ligand-independent. Indeed, ligand-independent endocytic recycling of receptors is not a novel phenomenon, which has been observed for G protein-coupled receptors (Leterrier *et al*, 2004; Xia *et al*, 2004; Trivedi & Bhattacharyya, 2012; Okamoto & Shikano, 2017), growth factor receptors (Knutson, 1992; Mitchell *et al*, 2004; Ioannou *et al*, 2017), scavenger receptor (Schaer *et al*, 2006), and receptor of the immunoglobulin superfamily (Qureshi *et al*, 2012). Like ligand-dependent endocytic recycling, constitutive recycling also mediates internalization of surface receptors into intracellular vesicles and subsequent trafficking back to the PM. In many cases, constitutive recycling encompasses clathrin-mediated endocytosis (Leterrier

et al, 2004; Mitchell *et al*, 2004; Xia *et al*, 2004; Qureshi *et al*, 2012; Okamoto & Shikano, 2017). It appears that there is not a major difference in the kinetics between ligand-dependent and -independent modes of endocytic recycling (Mitchell *et al*, 2004). Consistent with our results, Leterrier *et al* have shown that the ligand-independent endocytic recycling of the cannabinoid CB1 receptor expressed in HEK-293 cells is impaired by Rab4-S22N, but facilitated by Rab4-Q67L (Leterrier *et al*, 2004).

Notwithstanding, our study raises several open questions that require further investigations. First, apart from the LDLR, can AAS similarly increase the surface availability of other cargo receptors? Although our analysis on TfRs suggests that receptors lacking an excessive intracellular reserve in a putative slow recycling compartment are unlikely to be affected by AAS, and we have ruled out the involvement of LRP-1 and megalin/LRP-2, our study cannot exclude possible involvement of other cargo receptors in this process. Second, while our results suggest that the perinuclear pool of LDLRs might be involved in delivering receptors to the cell periphery under amino acid stress, yet the nature of this intracellular compartment is not clear. One possibility is that this part may represent the generic ERC or ERC-derived structures, based on the perinuclear location, the tubular morphology, and the partial colocalization with Rab11. However, we cannot rule out that this compartment represents specialized intracellular LDLR storage vesicles, similar to those for Glut4 in fat and muscle cells. Third, we do not understand how reducing the extracellular concentration of amino acids elevates the intracellular Ca^{2+} , although similar results have also been reported by other researchers (Ghislat *et al*, 2012).

The influence of dietary protein/amino acid restriction on systemic lipid metabolism is a topical research area (see the latest review article (Tricò *et al*, 2021)), with the available data being controversial and different views being under debate. Our *in vivo* data showing the overall long-term beneficial effect of dietary amino acid intervention on hypercholesterolemia in LDLR^{+/-} mice are in line with several recent studies (Henagan *et al*, 2016; Maida *et al*, 2018; Treviño-Villarreal *et al*, 2018). However, these results also suggest that such beneficial effects induced by dietary amino acid restriction are likely to involve multiple pathways such as lipogenesis (Treviño-Villarreal *et al*, 2018), fatty acid oxidation (Maida *et al*, 2018; Treviño-Villarreal *et al*, 2018) and/or autophagy (lipophagy) (Henagan *et al*, 2016). Hence, a limitation of this study was that we did not quantitatively determine the contribution of enhanced LDLR trafficking and LDL endocytosis in the overall anti-hypercholesterolemic effect of dietary amino acid restriction. The involvement of additional mechanisms is also supported by the observation that the total LDLR expression level was not reduced in the liver after amino acid restriction, because the increased cholesterol uptake is expected to repress LDLR expression via the SREBP2 pathway (Goldstein & Brown, 2009). These data indicate that the hepatic cells are not cholesterol-overloaded under the present experimental condition at least over the 3-day experimental period. Overall, our *in vitro* data and the acute AAS challenge results *in vivo* both support that AAS-stimulated cellular endocytosis of LDL may to some degree contribute to the long-term effects of dietary amino acid restriction on hypercholesterolemia by enhancing the clearance of LDL particles from the systemic circulation.

In summary, we have described a unique amino acid stress response, which directs the deployment of intracellular LDLRs, causing enhanced LDL endocytosis. This response appears to be mediated by Ca²⁺/CaMKII-Rab4 phosphorylation, leading to an increased abundance of LDLRs residing in the fast recycling route (Fig 8). At the cellular level, the stimulatory effect of AAS on LDL uptake is comparable to that induced by statins. At the systemic level, this response may facilitate LDLR-dependent clearance of LDL cholesterol from the circulation. We suggest that identification of signaling-controlled regulation of intracellular LDLR trafficking conceptually advances our understanding of the LDLR biology, and may benefit future development of additional therapeutic strategies for treating hypercholesterolemia. However, it should be stressed that upon amino acid restriction, multiple metabolic mechanisms may be activated and work in a coordinated manner to produce beneficial effects on systemic lipid metabolism *in vivo*.

Materials and Methods

Reagents and antibodies

Pitstop2 (ab120687) and Dynasore (ab120192) were purchased from Abcam (Cambridge, UK). Actinomycin D (S8964), BAPTA-AM (S7534), KN-93 (S7423), STO-609 (S8274), Cycloheximide (S7418), and pravastatin (S5713) were from Selleck Chemicals (Houston, TX, USA). MEM Vitamin solution (11120-052) and MEM Amino Acids Solution (11130077) were from Thermo Fisher (Waltham, MA, USA). Rapamycin (A8167), okadaic acid (A4540), leupeptin (A2570), and concanamycin A (A8633) were from APExBIO (Houston, TX, USA).

GCN2iB (HY-112654), A23187 (HY-N6687), and bafilomycin A1 (HY-100558) were from MedChemExpress (Monmouth Junction, NJ, USA). LDL (YB001) and DiI-LDL (YB0011) were from Yiyuan Biotechnology (Guangzhou, Guangdong Province, China). FITC-transferrin (009-090-050) was from Jackson ImmunoResearch (West Grove, Pennsylvania, USA). Alexa Fluor-488 conjugated Wheat Germ Agglutinin (W11261) was from Thermo Fisher. LysoTracker Red dye was purchased from Beyotime.

Antibodies for the following targets were used: LDLR (10785-1-AP, RRID:AB_2281164) (for western blot and immunofluorescence), Na-K ATPase (14418-1-AP, RRID:AB_2227873), LC3 (14600-1-AP, RRID:AB_2137737), Rab11 (20229-1-AP, RRID:AB_10666202), GFP (50430-2-AP, RRID:AB_11042881), GDI 1 (10249-1-AP, RRID:AB_2111520), Rabenosyn-5 (22218-1-AP, RRID:AB_11182179), p62/SQSTM1 (18420-1-AP, RRID:AB_10694431), vinculin (66305-1-Ig, RRID:AB_2810300), megalin/LDL receptor-related protein 2 (LRP2) (19700-1-AP, RRID:AB_10640428) (for immunofluorescence), β -actin (66009-1-Ig), GAPDH (60004-1-Ig), and COMMD1 (11938-1-AP, RRID:AB_2083542) were from Proteintech (Wuhan, Hubei Province, China). LDLR (AF2148, RRID:AB_2135126) (unconjugated goat IgG, for double immunofluorescence labeling of endogenous LDLR), LDLR (FAB2148P, RRID:AB_10573833) (PE-conjugated, for flow cytometry), megalin/LRP2 (FAB9578G) (for flow cytometry), and human apolipoprotein B (ApoB) (AF3556, RRID:AB_573025) were from R&D Systems (Minneapolis, MN, USA). LDLR (ab175883, for western blot only), Atg5 (ab108327, RRID:AB_2650499), EEA1 (ab2900, RRID:AB_2262056), Rab4 (ab108974, RRID:AB_10858141), Vps35 (ab10099, RRID:AB_296841), transferrin receptor (TfR) (ab84036, RRID:AB_10673794), p-(Ser/Thr) (ab17464, RRID:AB_443891), LDL receptor-related protein 1 (LRP1) (ab92544, RRID:AB_2234877, for immunofluorescence), GCN2 (ab134053, RRID:AB_2890925), and WASH1 (ab157592) were from Abcam. GDI α / β (E-5) (sc-374649, RRID:AB_11012027), p-CaMKII (sc-32289, RRID:AB_626786), CaMKII (sc-5306, RRID:AB_626788), and TfR (sc-32272, RRID:AB_627167, for double labeling experiments) were from Santa Cruz Biotechnology (Dallas, TX, USA). FLAG (8146S, RRID:AB_10950495), Rab5 (3547S, RRID:AB_2300649) and Rab7 (9367S, RRID:AB_1904103) were from Cell Signaling Technology (Danvers, MA, USA). LRP1 (12-0919-41) (for flow cytometry) was from eBioscience (San Diego, CA, USA).

Cell lines

HepG2 cells were purchased from National Collection of Authenticated Cell Cultures (Shanghai, China). The cells were cultured in Dulbecco's modified Eagle's medium (DMEM) supplemented with 10% fetal bovine serum (FBS), penicillin (100 U/ml), and streptomycin (100 μ g/ml) (all from Thermo Fisher), in an atmosphere with 5% CO₂. NIH-3T3 cells were purchased from ATCC (CRL-1658) (Manassas, VA, USA), and cultured in DMEM with 10% newborn calf serum (Biological Industries, Beit Haemek, Israel).

Animal studies

Male wild-type C57BL/6 mice and LDLR^{-/-} mice (6–8 weeks of age) were purchased from Vital River Laboratories (Beijing, China). The use of experimental animals, dietary interventions, and sample collection procedures were reviewed and approved by the

Institutional Animal Ethics Committee of Shandong University, and carried out in accordance with the Guide for Care and Use of Laboratory Animals (NIH, 1996). Animals were maintained in sterilized, mechanically ventilated polycarbonate cages (4–5 mice per cage) with corn cob bedding, within a standardized housing facility (non-SPF), on normal chow diet and sterilized tap water *ad lib* until 8–10 weeks of age (weighing 18–22 g). The ARRIVE guidelines were consulted for reporting results from the *in vivo* experiments.

Isolation of primary hepatocytes and stromal vascular fraction

Mice were euthanized by intraperitoneal injection of overdose of pentobarbital sodium, and the liver was perfused via vena cava cannulation with prewarmed Hank's Balanced Salt Solution (HBSS, with $\text{Ca}^{2+}/\text{Mg}^{2+}$) containing 0.5 mg/ml collagenase type II (from Solarbio, Beijing, China) for 5 min. Then the partially digested liver was removed into a culture dish, minced, and further digested in the same buffer until complete disintegration of the tissue blocks. Liberated cells were filtered through a 100- μm cell strainer, and centrifuged in 40% percoll (from Solarbio) at 200 g for 15 min. The hepatocytes were resuspended and plated in DMEM with 10% FBS. The attached cells were used for experimentation within 24 h. The stromal vascular fraction (SVF) was prepared using inguinal white adipose tissues. Briefly, adipose was finely minced and digested using a solution containing 1 mg/ml collagenase type II in PBS for 1 h at 37°C. The digestion reaction was stopped with DMEM/F12 (Thermo Fisher) containing 10% FBS. After passing through the cell strainer, cells were collected by centrifugation at 1,000 rpm for 10 min, and maintained in complete DMEM/F12 medium with 2 mM of L-glutamine and antibiotic/antimycotic mixture (A5955, Sigma-Aldrich, St. Louis, MO, USA). Cells were maintained in 75- cm^2 flasks until 80% confluent and used for experimentation.

Amino acid starvation (AAS) treatment and replenishment experiment

Complete DMEM containing 10% FBS and 2 mM of L-glutamine was defined as the normal medium containing 100% amino acids. HBSS (with $\text{Ca}^{2+}/\text{Mg}^{2+}$) supplemented with 10% FBS and Gibco MEM Vitamin Solution (11120052, Thermo Fisher) was used as the AAS (0% amino acids) medium. Mediums containing 25, 50, and 75% amino acids were prepared by combining the above two solutions with varying proportions. For amino acids replenishment experiments, MEM Amino Acids Solution (11130051, Thermo Fisher) and 2 mM of L-glutamine were added into the AAS (0%) medium.

DiI-LDL fluorescence microscopy and spectrometry

The cells cultured on chamber slides were washed and incubated with DiI-LDL (from Yiyuan Biotechnology, Guangzhou, China) at 10 $\mu\text{g}/\text{ml}$ for different time intervals as indicated. The cells were then washed thoroughly, chilled on ice, and briefly fixed with 4% paraformaldehyde. DiI fluorescence was detected using a confocal microscope (Model LSM710, Zeiss, Jena, Germany) under excitation 550 nm and emission 590 nm, or a fluorescent microscope (Eclipse Ni-U, Nikon, Japan) equipped with a TRITC band-pass filter. For each slide, 3 to 5 high power fields were randomly selected and the mean fluorescent intensity was measured cell-by-cell using ImageJ

software (NIH). The averaged intensity values were used as the final data. Fluorescent image analysis was performed in a blind manner.

In some experiments, DiI-LDL fluorescence was measured by spectrometry. The cells were initially seeded in 12-well plates at a density of 5×10^5 cells/ml for overnight. After incubation with DiI-LDL for varying time intervals as indicated, the cells were chilled by washing three times with cold PBS containing 5 mg/ml of bovine serum albumin. Then the cells were washed with cold PBS containing 1 mg/ml of bovine serum albumin plus 25 mM of acetic acid (pH 4.2) to remove residual LDL on the cell surface. Finally, the cells were detached with trypsin, and aliquots of equal amount of the cell suspension were transferred to an opaque 96-well plate. Fluorescence intensity was measured using SpectraMax Gemini XPS microplate reader (Molecular Devices, Sunnyvale, CA, USA), at excitation 549 nm and emission 565 nm.

Cellular cholesterol measurement

Cellular cholesterol content was assayed using Tissue Total Cholesterol Assay kit (E1026, from Applygen Technologies, Beijing, China), according to the manufacturer's protocol. The endpoint was determined by measuring absorbance at 550 nm using EMax Plus microplate reader (Molecular Devices). The raw data were normalized with total protein concentrations.

Immunoprecipitation and western blot

The cells were homogenized in cold lysis buffer containing 100 mM of NaCl, 2 mM of MgCl_2 , 1% Triton X-100, 20 mM of HEPES (pH 7.4), and Protease Inhibitor Mixture (P1260, from Solarbio). For immunoprecipitation, samples were adjusted to a protein concentration of 0.5 or 1.0 mg/ml, precleared with normal IgG and Protein A/G agarose beads (from Cell Signaling Technology), and incubated with primary antibodies at 4°C for 4 h. Then the samples were mixed with Protein A/G beads and further incubated at 4°C for overnight with constant rotation. The beads were washed, and bound proteins were eluted by boiling in Laemmli loading buffer. For plasma membrane purification, a commercial kit from Invent Biotechnologies (SM-005) (Beijing, China) was used. For western blotting, samples were separated by SDS/PAGE and transferred to PVDF membranes. The membrane was blocked with 5% nonfat milk, incubated with specific primary antibodies overnight, followed by incubation with horseradish peroxidase-conjugated secondary antibodies. The membrane was developed with ECL Prime Reagent (from Merck Millipore, Darmstadt, Germany), and signals were detected using a luminescent image analyzer (ChemiDoc XRS+, Bio-Rad, Hercules, CA, USA). Band densitometry analysis was performed using ImageJ.

Membrane surface protein biotinylation and pull-down experiments

To label cell surface proteins at the steady state, NIH-3T3 cells were grown in 10-cm plates to ~80% confluence. After various treatments, cells were washed three times with cold PBS and chilled on ice for 15 min. Surface proteins were labeled by a noncleavable biotin conjugation reaction using Cell Surface Protein Isolation Kit (#K295-10, from BioVision, Milpitas, CA, USA) according to the

manufacturer's instructions. Biotin-conjugated proteins were precipitated by incubating (with rotation) the cell homogenates with Streptavidin Sepharose beads (from BioVision) at 4°C for overnight. The beads were subject to western blot analysis as described above. To examine the rate of LDLR internalization and recycling to PM, surface biotin-disulfide pulse-chase labeling experiments were conducted as described (Gu *et al*, 2010), using a water-soluble, disulfide-reducible Sulfo-NHS-SS-Biotin protein biotinylation kit (#2323-100, from BioVision) as instructed. Briefly, the cells were incubated with 0.5 mM Sulfo-NHS-SS-Biotin reagent at 4°C for 30 min. Excess reagent was quenched with 50 mM of NH₄Cl. After three washes to eliminate free biotin, the cells were either kept at 4°C (background), or shifted to 37°C for varying time intervals. At the end of the procedure, the cells were chilled at 4°C and incubated with cold glutathione solution (50 mM) for 2 times 15 min. The cells were solubilized in RIPA buffer and subject to Streptavidin Sepharose pull-down analysis as described above.

In vitro phosphorylation assay

A FLAG-tagged short peptide spanning a.a.120–154 of murine Rab4a, termed Rab4a (120–154), and the corresponding 137T-to-A mutant, were synthesized (from LC-BIO Technologies Co. Ltd., Hangzhou, Zhejiang province, China). Recombinant human CaMKII α (ab60899, from Abcam) was activated in a kinase buffer (containing 50 mM of Tris-HCl, pH 7.5, 10 mM of MgCl₂, 0.1 mM of EDTA, 2 mM of dithiothreitol, and 0.01% Brij-35) supplemented with 200 μ M of ATP (from New England Biolabs, Ipswich, MA, USA), 1.2 μ M of calmodulin (ab189137, from Abcam), and 2 mM of CaCl₂. The reaction was initiated by incubating the mixture at 30°C for 15 min, and terminated by cooling on ice. Negative control experiment was conducted by omitting calmodulin and CaCl₂ in the reaction mixture. *In vitro* phosphorylation was carried out by mixing 50 μ M of substrate peptide, 200 μ M of ATP, and 3 μ g of CaMKII in the kinase buffer (total volume 100 μ l). The reaction was initiated by incubating at 30°C for 15 min, and terminated by addition of Laemmli loading buffer. The samples were boiled and analyzed by SDS-PAGE and western blot.

Immunofluorescence and fluorescence recovery after photobleaching (FRAP)

For immunofluorescence, the cells cultured on glass slides were fixed in cold methanol, permeabilized with 0.1% Triton X-100, and blocked with 1% albumin. The cells were incubated with diluted primary antibodies at 4°C for overnight, followed by incubation with fluorophore-conjugated secondary antibodies (from Proteintech) at room temperature for 2 h. To specifically label LDLRs on the plasma membrane, the cells were briefly fixed with 4% paraformaldehyde without permeabilization, blocked, and incubated with primary anti-LDLR antibody (10785-1-AP from Proteintech). Then the slides were sequentially labeled with biotinylated secondary antibody and Alexa Fluor 594-conjugated streptavidin (016-580-084, RRID: AB_2337250, from Jackson ImmunoResearch). Slides were counterstained with DAPI. For each slide, 3 to 5 random high-power fields were selected for analysis. Fluorescent images were taken using the Zeiss confocal microscope. Fluorescence intensity profile analysis was performed using the Plot Profile tool in

ImageJ. For quantitative assessment of co-localization of the dual-color signals obtained in double immuno-labeling experiments, Manders Overlap Coefficient values were calculated using ZEN software suite (Zeiss) (Manders *et al*, 1993). Immuno-fluorescence images were measured in an operator-blind manner.

FRAP assays were performed using the LSM710 Zeiss confocal microscope. The cells transfected with GFP-LDLR were seeded in 35-mm glass bottom dishes. The cells were observed with a 63 \times oil immersion objective lens (Apo NA1.4) using the following settings: 5% laser power at 488 nm, gain value 750, pinhole size 1.57 Airy Units. Five prebleach images (512 \times 512) were captured at a scan speed of 780 ms/frame. Photo bleaching of the region-of-interest was performed by irradiating with 100% laser power and 6.3 μ s of pixel dwell time for 10 iterations. A series of postbleach images of the whole cell were acquired with low power illumination at a frequency of 1 frame per second over a duration of 2 min. The fluorescence recovery rate was determined using the following formula: (Postbleach intensity - Background)/(Prebleach intensity - Background) \times 100%, where Background was the fluorescence intensity value immediately after photo bleaching.

Flow cytometry

To detect DiI-LDL internalization, the cells were chilled on ice, washed thoroughly with cold PBS, and detached with trypsin. The resuspended cells were fixed with 4% paraformaldehyde for 20 min on ice, and analyzed with a Cytomics FC 500 cytometer (Beckman Coulter, Brea, CA, USA). For LDLR labeling, detached cells were fixed and labeled either indirectly with unconjugated primary LDLR antibody followed by FITC-conjugated anti-IgG, or directly with PE-conjugated primary LDLR antibody. Data were analyzed using FlowJo software (Becton, Dickinson and Company, Franklin Lakes, NJ, USA).

Intracellular Ca²⁺ imaging

The cells were plated in 35-mm glass bottom dishes, and loaded with 2 μ M of Fluo-3AM (from Beyotime) for 30 min at 37°C. Fluorescence signals were detected using the Zeiss confocal microscope at 488-nm excitation and 530-nm emission. Image processing and analysis were performed using ZEN 2009 Light Edition software (from Zeiss).

Quantitative real-time PCR (qPCR)

Total RNA was extracted using TRIzol Reagent (Thermo Fisher). Total RNA of 2 μ g was reverse transcribed to cDNA using PrimeScript RT Reagent Kit (Takara, Shiga, Japan). PCR amplification was performed using Forget-Me-Not EvaGreen qPCR Master Mix (High ROX) (Biotium, Fremont, CA, USA) in a StepOnePlus qPCR system (Thermo Fisher). The primer sequences were listed in Appendix Table S2. The raw data were normalized using 2^{- $\Delta\Delta$ Ct} method. GAPDH or β -actin was used as the housekeeping gene.

Gene silencing by siRNA

Chemically modified (2'-OMe) siRNA molecules targeting human Atg5, murine GCN2, and human Rab4a were purchased from

Genepharma (Shanghai, China) (for sequences see Appendix Table S2). A nontargeting sequence was used as control. Transfection of siRNA was performed using Lipofectamine RNAiMAX Transfection Reagent (from Thermo Fisher) with a final concentration of siRNA of 30 nM. The cells were used for experiments 48 h after transfection.

Plasmid transfection and site-directed mutagenesis

All of the plasmids used in the study were obtained from Addgene (Watertown, MA, USA). GFP-LDLR (#98184; RRID: Addgene_98184) was a gift from Gary Banker & Marvin Bentley (Jenkins *et al*, 2012). EGFP-Rab4a (#49434; RRID: Addgene_49434), EGFP-Rab4a-Q67L (#49475; RRID: Addgene_49475), and EGFP-Rab4a-S22N (#49476; RRID: Addgene_49476) were gifts from Marci Scidmore (Rzomp *et al*, 2003). Rab4a-T137A mutant was generated using Q5 Site-Directed Mutagenesis Kit (from New England Biolabs), and the mutation was confirmed by sequencing. Plasmid transfections were performed using Lipofectamine 3000 according to the manufacturer's instructions.

In vivo dietary amino acid interventions

For all animal experiments, subject selection for different test groups was carried out in a random manner. For acute AAS challenge experiments, wild-type mice were first adapted to a control diet (D12450B, from Research Diets, New Brunswick, NJ, USA), in which 20% of the total calories were from protein, for 7 days. Then the animals were switched to a calorie-matched amino acid-free diet (D12051001, Research Diets) (starting from 10 AM), for up to 72 h. Two hours before the end of experiment, mice were infused with DiI-LDL (5 mg/kg, resuspended in saline) via the tail vein. The mice were anesthetized by intraperitoneal injection of pentobarbital sodium (60 mg/kg) and killed by cardiac bleeding; the systemic circulation was flushed with cold saline via left ventricle, and the livers were removed. A part of the liver samples were embedded in OCT medium, and snap frozen in liquid nitrogen. For fluorescence microscopy detection of DiI-LDL, frozen sections of 10- μ m thickness were cut. The remaining liver tissues were snap frozen and stored at -80°C for biochemical analyses. To assess the clearance rate of infused DiI-LDL from the systemic circulation, DiI-LDL was infused at a dose of 10 mg/kg. At different time points as indicated, retro-orbital blood samples were collected under general anesthesia. DiI fluorescence intensity in the plasma was measured using the SpectraMax Gemini XPS microplate reader (200 μ l per well).

For long-term dietary amino acid restriction experiments, *LDLR*^{+/-} mice were fed with a high-fat (HF), amino acid-sufficient diet (HF/AA100%), which was prepared by mixing a HF diet containing 21% lard and 1% cholesterol (from Keao Xieli Feed Co., Beijing, China), and the D12450B diet (see above) in 1:1; or a HF amino acid-restricted diet (HF/AA50%), in which the content of amino acids was reduced to 50% by mixing the HF diet and the D12051001 diet in 1:1. The dieting treatment was continued for 4 weeks. At week 2, blood samples were obtained via retro-orbital puncture under general anesthesia. At week 4, mice were anesthetized with pentobarbital and killed by right atrial puncture and bleeding. Blood samples were collected for cholesterol measurements. Except for technical procedural failures, no subjects were excluded from final data analysis.

Blood cholesterol measurements

Serum total cholesterol and LDL cholesterol levels were determined using commercial assay kits (#E1005 and #E1018, respectively, from Applygen, Beijing, China). Fast protein liquid chromatography (FPLC) analysis of plasma lipoproteins was performed as described (Guo *et al*, 2018). Briefly, pooled plasma aliquots (200 μ l from each group) were applied to Tricorn high-performance Superose S-6 10/300GL columns and filtered using an Amersham FPLC system (GE Healthcare, Chicago, IL, USA), followed by elution with PBS at a constant flow rate of 0.25 ml/min. Eluted fractions (500 μ l per fraction) were assessed for cholesterol concentrations using enzymatic assay (Guo *et al*, 2018). FPLC was carried out in an investigator-blind manner.

Data and statistics

Data were expressed as mean \pm standard deviation (SD). Statistical analyses were performed with unpaired *t*-test (for 2 groups) or one-way analysis of variance (ANOVA) with *post hoc* Tukey's test (for multiple comparisons). Prism (Version 8.0) from GraphPad Software (San Diego, CA, USA) (RRID:SCR_002798) was used for statistical analysis. No outliers were excluded from the final data analysis. A *P* value of < 0.05 (two-tailed) was considered to be significant. The declared group size and the data points in graphs represented independent values but not technical replicates. The minimum *n* number for general biological assays was determined to be 4–5 as calculated using an online tool at "<https://www.stat.ubc.ca/~rollin/stats/ssize/n2.html>", with estimated values of 40% mean difference and 20% variance. At least *n* = 5 animals per group were included for *in vivo* tests. For some tests with a large mean difference and low variance, *n* = 3 might be included if the *P* value reached significance. Some data from basic characterization tests with *n* = 2 were clearly labeled as "preliminary" and not subjected to statistical analysis. Parametric tests were used if the data passed at least one of the following normality tests: Anderson–Darling, D'Agostino–Pearson omnibus, Shapiro–Wilk, and Kolmogorov–Smirnov. Otherwise the data were analyzed with nonparametric tests, which were specified in the figure legends. Parametric tests were performed assuming there were equal variances. The sample size for all treatment groups was predetermined to be the same to minimize the potential impact of variance inequality on statistical results.

Data availability

This study includes no data deposited in external repositories.

Expanded View for this article is available online.

Acknowledgments

The authors thank Dr. Yuhui Wang (Institute of Cardiovascular Sciences, Peking University) for technical assistances with FPLC assays; Ms Xinyun Li and Ms Mi Tian (Qilu Hospital of Shandong University) for assistances with confocal microscopy and western blot experiments. This work was partially supported by the following grants: National Natural Science Foundation of China (82070265, 81770469 for F.J.; 81920108003, 81770442,

82030051 for C.Z.), Major Projects of National Science and Technology of China (2012ZX09303016-003 for H.G.), Program of Introducing Talents of Discipline to Universities (No. BP0719033 for C.Z.), and Taishan Scholar Project of Shandong Province of China (for C.Z.).

Author contributions

Ye Chen: Data curation; Formal analysis; Investigation; Writing – original draft; Writing – review & editing. **Xiao Wu:** Data curation; Formal analysis; Investigation; Writing – review & editing. **Jing Zhang:** Data curation; Investigation. **Guopin Pan:** Data curation; Investigation. **Xiaoyun Wang:** Data curation; Investigation. **Xiaosun Guo:** Data curation; Formal analysis; Investigation. **Jianli Wang:** Data curation; Formal analysis. **Xiaopei Cui:** Data curation; Formal analysis; Investigation. **Haiqing Gao:** Formal analysis; Funding acquisition. **Mei Cheng:** Formal analysis. **Jingwen Yang:** Data curation; Investigation. **Cheng Zhang:** Formal analysis; Supervision; Funding acquisition; Project administration; Writing – review & editing. **Fan Jiang:** Conceptualization; Formal analysis; Supervision; Funding acquisition; Writing – original draft; Project administration; Writing – review & editing.

In addition to the CRediT author contributions listed above, the contributions in detail are YC, X. Wu, JZ, GP, X. Wang, XG, XC, and JY contributed to experimentation, data acquisition, and raw data processing; YC, X. Wu, XG, JW, HG, MC, CZ, and FJ contributed to experimental design, data analysis, and/or data interpretation; YC, X. Wu, FJ, and CZ contributed to manuscript drafting, editing, revising, and/or final approval; FJ, CZ, and HG contributed to funding acquisition and management; FJ conceived the study.

Disclosure statement and competing interests

The authors declare that they have no conflict of interest.

References

- Anthony TG, Morrison CD, Gettys TW (2013) Remodeling of lipid metabolism by dietary restriction of essential amino acids. *Diabetes* 62: 2635–2644
- Arjonen A, Alanko J, Veltel S, Ivaska J (2012) Distinct recycling of active and inactive β 1 integrins. *Traffic* 13: 610–625
- Bartuzi P, Billadeau DD, Favier R, Rong S, Dekker D, Fedoseienko A, Fieten H, Wijers M, Levels JH, Huijman N et al (2016) CCC- and WASH-mediated endosomal sorting of LDLR is required for normal clearance of circulating LDL. *Nat Commun* 7: 10961
- Bryant NJ, Govers R, James DE (2002) Regulated transport of the glucose transporter GLUT4. *Nat Rev Mol Cell Biol* 3: 267–277
- Burden JJ, Sun XM, García AB, Soutar AK (2004) Sorting motifs in the intracellular domain of the low density lipoprotein receptor interact with a novel domain of sorting nexin-17. *J Biol Chem* 279: 16237–16245
- Carroll B, Korolchuk VI, Sarkar S (2015) Amino acids and autophagy: cross-talk and co-operation to control cellular homeostasis. *Amino Acids* 47: 2065–2088
- Castilho BA, Shanmugam R, Silva RC, Ramesh R, Himme BM, Sattlegger E (2014) Keeping the eIF2 alpha kinase Gcn2 in check. *Biochim Biophys Acta* 1843: 1948–1968
- Cormont M, Tanti JF, Zahraoui A, Van Obberghen E, Le Marchand-Brustel Y (1994) Rab4 is phosphorylated by the insulin-activated extracellular-signal-regulated kinase ERK1. *Eur J Biochem* 219: 1081–1085
- Ghislát G, Patron M, Rizzuto R, Knecht E (2012) Withdrawal of essential amino acids increases autophagy by a pathway involving Ca^{2+} /calmodulin-dependent kinase kinase- β (CaMKK- β). *J Biol Chem* 287: 38625–38636
- Goldstein JL, Brown MS (2009) The LDL receptor. *Arterioscler Thromb Vasc Biol* 29: 431–438
- Grant BD, Donaldson JG (2009) Pathways and mechanisms of endocytic recycling. *Nat Rev Mol Cell Biol* 10: 597–608
- Gu J, Faundez V, Werner E (2010) Endosomal recycling regulates Anthrax Toxin Receptor 1/Tumor Endothelial Marker 8-dependent cell spreading. *Exp Cell Res* 316: 1946–1957
- Guo X, Gao M, Wang Y, Lin X, Yang L, Cong N, An X, Wang F, Qu K, Yu L et al (2018) LDL receptor gene-ablated hamsters: a rodent model of familial hypercholesterolemia with dominant inheritance and diet-induced coronary atherosclerosis. *EBioMedicine* 27: 214–224
- Heeren J, Beisiegel U (2001) Intracellular metabolism of triglyceride-rich lipoproteins. *Curr Opin Lipidol* 12: 255–260
- Henagan TM, Laeger T, Navard AM, Albarado D, Noland RC, Stadler K, Elks CM, Burk D, Morrison CD (2016) Hepatic autophagy contributes to the metabolic response to dietary protein restriction. *Metabolism* 65: 805–815
- Hu J, Zhang Z, Shen WJ, Azhar S (2010) Cellular cholesterol delivery, intracellular processing and utilization for biosynthesis of steroid hormones. *Nutr Metab* 7: 47
- Ioannou MS, Kulasekaran G, Fotouhi M, Morein JJ, Han C, Tse S, Nossova N, Han T, Mannard E, McPherson PS (2017) Intersectin-s interaction with DENND2B facilitates recycling of epidermal growth factor receptor. *EMBO Rep* 18: 2119–2130
- Jenkins B, Decker H, Bentley M, Luisi J, Banker G (2012) A novel split kinesin assay identifies motor proteins that interact with distinct vesicle populations. *J Cell Biol* 198: 749–761
- Jewell JL, Guan KL (2013) Nutrient signaling to mTOR and cell growth. *Trends Biochem Sci* 38: 233–242
- Karusheva Y, Koessler T, Strassburger K, Markgraf D, Mastrototaro L, Jelenik T, Simon M-C, Pesta D, Zaharia O-P, Bódis K et al (2019) Short-term dietary reduction of branched-chain amino acids reduces meal-induced insulin secretion and modifies microbiome composition in type 2 diabetes: a randomized controlled crossover trial. *Am J Clin Nutr* 110: 1098–1107
- Knutson VP (1992) Ligand-independent internalization and recycling of the insulin receptor. Effects of chronic treatment of 3T3-C2 fibroblasts with insulin and dexamethasone. *J Biol Chem* 267: 931–937
- Leterrier C, Bonnard D, Carrel D, Rossier J, Lenkei Z (2004) Constitutive endocytic cycle of the CB1 cannabinoid receptor. *J Biol Chem* 279: 36013–36021
- Leto D, Saltiel AR (2012) Regulation of glucose transport by insulin: traffic control of GLUT4. *Nat Rev Mol Cell Biol* 13: 383–396
- Liu W, Yuen EY, Yan Z (2010) The stress hormone corticosterone increases synaptic alpha-amino-3-hydroxy-5-methyl-4-isoxazolepropionic acid (AMPA) receptors via serum- and glucocorticoid-inducible kinase (SGK) regulation of the GDI-Rab4 complex. *J Biol Chem* 285: 6101–6108
- Maida A, Zota A, Vegiopoulos A, Appak-Baskoy S, Augustin HG, Heikenwalder M, Herzig S, Rose AJ (2018) Dietary protein dilution limits dyslipidemia in obesity through FGF21-driven fatty acid clearance. *J Nutr Biochem* 57: 189–196
- Manders EMM, Verbeek FJ, Aten JA (1993) Measurement of co-localization of objects in dual-colour confocal images. *J Microsc* 169: 375–382
- Maxfield FR, McGraw TE (2004) Endocytic recycling. *Nat Rev Mol Cell Biol* 5: 121–132
- Mitchell H, Choudhury A, Pagano RE, Leaf EB (2004) Ligand-dependent and -independent transforming growth factor-beta receptor recycling regulated by clathrin-mediated endocytosis and Rab11. *Mol Biol Cell* 15: 4166–4178
- Mourikis P, Zako S, Dannenberg L, Nia AM, Heinen Y, Busch L, Richter H, Hohlfeld T, Zeus T, Kelm M et al (2020) Lipid lowering therapy in

- cardiovascular disease: From myth to molecular reality. *Pharmacol Ther* 213: 107592
- Naslavsky N, Caplan S (2018) The enigmatic endosome - sorting the ins and outs of endocytic trafficking. *J Cell Sci* 131: jcs216499
- Okamoto Y, Shikano S (2017) Differential phosphorylation signals control endocytosis of GPR15. *Mol Biol Cell* 28: 2267–2281
- Qureshi OS, Kaur S, Hou TZ, Jeffery LE, Poulter NS, Briggs Z, Kenefick R, Willox AK, Royle SJ, Rappoport JZ et al (2012) Constitutive clathrin-mediated endocytosis of CTLA-4 persists during T cell activation. *J Biol Chem* 287: 9429–9440
- Ravikumar B, Sarkar S, Davies JE, Futter M, Garcia-Arencibia M, Green-Thompson ZW, Jimenez-Sanchez M, Korolchuk VI, Lichtenberg M, Luo S et al (2010) Regulation of mammalian autophagy in physiology and pathophysiology. *Physiol Rev* 90: 1383–1435
- de Renzis S, Sönnichsen B, Zerial M (2002) Divalent Rab effectors regulate the sub-compartmental organization and sorting of early endosomes. *Nat Cell Biol* 4: 124–133
- Rzomp KA, Scholtes LD, Briggs BJ, Whittaker GR, Scidmore MA (2003) Rab GTPases are recruited to chlamydial inclusions in both a species-dependent and species-independent manner. *Infect Immun* 71: 5855–5870
- Schaer CA, Schoedon G, Imhof A, Kurrer MO, Schaer DJ (2006) Constitutive endocytosis of CD163 mediates hemoglobin-heme uptake and determines the noninflammatory and protective transcriptional response of macrophages to hemoglobin. *Circ Res* 99: 943–950
- van der Sluijs P, Hull M, Huber LA, Mâle P, Goud B, Mellman I (1992) Reversible phosphorylation–dephosphorylation determines the localization of rab4 during the cell cycle. *EMBO J* 11: 4379–4389
- van de Sluis B, Wijers M, Herz J (2017) News on the molecular regulation and function of hepatic low-density lipoprotein receptor and LDLR-related protein 1. *Curr Opin Lipidol* 28: 241–247
- Songyang Z, Lu KP, Kwon YT, Tsai LH, Filhol O, Cochet C, Brickey DA, Soderling TR, Bartleson C, Graves DJ et al (1996) A structural basis for substrate specificities of protein Ser/Thr kinases: primary sequence preference of casein kinases I and II, NIMA, phosphorylase kinase, calmodulin-dependent kinase II, CDK5, and Erk1. *Mol Cell Biol* 16: 6486–6493
- Stenmark H (2009) Rab GTPases as coordinators of vesicle traffic. *Nat Rev Mol Cell Biol* 10: 513–525
- Treviño-Villarreal JH, Reynolds JS, Bartelt A, Langston PK, MacArthur MR, Arduini A, Tosti V, Veronese N, Bertozzi B, Brace LE et al (2018) Dietary protein restriction reduces circulating VLDL triglyceride levels via CREBH-APOA5-dependent and -independent mechanisms. *JCI Insight* 3: e99470
- Tricò D, Biancalana E, Solini A (2021) Protein and amino acids in nonalcoholic fatty liver disease. *Curr Opin Clin Nutr Metab Care* 24: 96–101
- Trivedi RR, Bhattacharyya S (2012) Constitutive internalization and recycling of metabotropic glutamate receptor 5 (mGluR5). *Biochem Biophys Res Commun* 427: 185–190
- Vos D, Kuivenhoven JA, van de Sluis B (2018) Recycling the LDL receptor to combat atherosclerosis. *Aging* 10: 3638–3640
- White RR, Kwon YG, Taing M, Lawrence DS, Edelman AM (1998) Definition of optimal substrate recognition motifs of Ca²⁺-calmodulin-dependent protein kinases IV and II reveals shared and distinctive features. *J Biol Chem* 273: 3166–3172
- Wijers M, Kuivenhoven JA, van de Sluis B (2015) The life cycle of the low-density lipoprotein receptor: insights from cellular and *in vivo* studies. *Curr Opin Lipidol* 26: 82–87
- Xia S, Kjaer S, Zheng K, Hu P-S, Bai L, Jia J-Y, Rigler R, Pramanik A, Xu T, Hokfelt T et al (2004) Visualization of a functionally enhanced GFP-tagged galanin R2 receptor in PC12 cells: constitutive and ligand-induced internalization. *Proc Natl Acad Sci U S A* 101: 15207–15212
- Xiao Y, Rabien A, Buschow R, Amtslavskiy V, Busch J, Kilic E, Villegas SL, Timmermann B, Schütte M, Mielke T et al (2020) Endocytosis-mediated replenishment of amino acids favors cancer cell proliferation and survival in chromophobe renal cell carcinoma. *Cancer Res* 80: 5491–5501
- Yap YW, Rusu PM, Chan AY, Fam BC, Jungmann A, Solon-Biet SM, Barlow CK, Creek DJ, Huang C, Schittenhelm RB et al (2020) Restriction of essential amino acids dictates the systemic metabolic response to dietary protein dilution. *Nat Commun* 11: 2894
- Yu D, Richardson NE, Green CL, Spicer AB, Murphy ME, Flores V, Jang C, Kasza I, Nikodemova M, Wakai MH et al (2021) The adverse metabolic effects of branched-chain amino acids are mediated by isoleucine and valine. *Cell Metab* 33: 905–922



License: This is an open access article under the terms of the Creative Commons Attribution-NonCommercial-NoDeriv License, which permits use and distribution in any medium, provided the original work is properly cited, the use is non-commercial and no modifications or adaptations are made.